Mon. Not. R. Astron. Soc. **366,** 865–883 (2006) doi:10.1111/j.1365-2966.2005.09973.x

The core of the Canis Major galaxy as traced by red clump stars

M. Bellazzini,[1⋆] R. Ibata,[2] N. Martin,[2] G. F. Lewis,[3] B. Conn[3] and M. J. Irwin[4]

[1]*INAF – Osservatorio Astronomico di Bologna, via Ranzani 1, 40127, Bologna, Italy*
[2]*Observatoire de Strasbourg, 11, rue de l'Université, F-67000, Strasbourg, France*
[3]*Institute of Astronomy, School of Physics, A29, University of Sydney, NSW 2006, Australia*
[4]*Institute of Astronomy, Madingley Road, Cambridge CB3 0HA*

Accepted 2005 November 18. Received 2005 November 3; in original form 2005 April 21

ABSTRACT

The recently discovered stellar system in Canis Major is analysed using He-burning red clump stars as tracers. Canis Major turns out to be the strongest and the most spatially confined overdensity of the whole Galactic disc, in terms of both number density and statistical significance. When projected on to the Galactic plane, it appears as an elongated and compact overdensity extending from $l \sim 200^\circ$ to 280° with a roundish core towards $l \sim 240^\circ$. We find that the main body of the system has an integrated absolute magnitude $M_V = -14.4 \pm 0.8$, a central surface brightness $\mu_{V,0} \simeq 24.0 \pm 0.6$ and a line-of-sight (LOS) profile peaked at $D_\odot = 7.2 \pm 1.0$ kpc with half width at half maximum ~ 2.0 kpc, in excellent agreement with the results obtained with widely different tracers (M giants and main-sequence stars) in previous analyses. The mean distance to the main body of Canis Major is observed to increase with increasing Galactic longitude, from $D_\odot \simeq 6.3$ kpc at $l \simeq 225^\circ$ to $D_\odot \simeq 9.3$ kpc at $l \simeq 265^\circ$, in good agreement with the predictions of our more recent N-body simulation that models Canis Major (CMa) as a dwarf galaxy being accreted in a planar orbit on to the disc of the Milky Way. We confirm that the Canis Major system has all the characteristics of the relic of a dwarf galaxy seen on top of a large-scale overdensity that we detect all over the third and fourth Galactic quadrants ($180^\circ \leqslant l \leqslant 360^\circ$, with a strong maximum around $l = 290^\circ$ and $b \gtrsim -5^\circ$) that is identified as the stellar component of the Southern Galactic warp. On the other hand, the possibility that a peculiar deformation/asymmetry of the outer Galactic disc may be at the origin of the observed distribution of overdensities towards CMa cannot be definitely ruled out with the data presented in this paper. We also address a recent claim that Canis Major is on the outskirts of a larger 'Argo' structure centred at $l \simeq 290^\circ$. Our analysis shows that the stellar populations in the latter are distributed over a very large distance range along the LOS, and do not give rise to a narrow peak in density in this direction, contrary to what is observed in Canis Major. This suggests that the Argo structure is likely due to Galactic asymmetries such as the warp.

Key words: open clusters and associations: general – open clusters and associations: individual: Tombaugh 2, AM-2, Heffner 11 – galaxy: structure – galaxies: dwarf.

1 INTRODUCTION

During the last decade, it has been fully realized that the relics of the latest accretion events that contributed to the assembly of the Milky Way can be observationally identified and studied in detail (see e.g. Ibata et al. 2001; Newberg et al. 2002; Majewski et al. 2003, and references therein). These findings simultaneously provide a qualitative confirmation and a new challenge for the current cosmological models in which the growth of large galaxies is driven by the process of hierarchical merger of subunits (White & Rees 1978; White & Frenk 1991). The tidal disruption of dwarf galaxies within the Galactic potential may lead to the production of long-lived stellar streams (as in the case of the dwarf spheroidal Sagittarius galaxy – Sgr dSph; see Ibata & Lewis 1998; Ivezic et al. 2000; Ibata et al. 2001, 2002; Newberg et al. 2002; Majewski et al. 2003; Bellazzini, Ferraro & Ibata 2003a) that may reveal fundamental information about the process of disruption, the mass distribution within the Galactic halo of dark matter, its degree of clumpiness, etc. (see Ibata et al. 2001; Helmi 2004; Johnston, Law & Majewski 2005; Law, Johnston & Majewski 2005).

The recent discovery of a large stellar stream nearly coplanar with the Galactic disc (the Canis Major/Monoceros Ring, hereafter the

⋆E-mail: michele.bellazzini@bo.astro.it

Ring, for brevity; Newberg et al. 2002; Yanny et al. 2003; Ibata et al. 2003; Majewski et al. 2003; Rocha-Pinto et al. 2003; Crane et al. 2003; Conn et al. 2005a,b) suggests that the accretion of small stellar systems may have had a considerable rôle also in the assembly of the disc components of the Milky Way (in particular, the thick disc) as envisaged by the latest detailed models of disc-galaxy formation within a cosmological context (Abadi et al. 2003a,b; Helmi, White & Springel 2003).

In Martin et al. (2004a, hereafter Paper I), we reported on the identification of a possible new stellar relic (the Canis Major dwarf galaxy, hereafter CMa) located at 7–8 kpc from the Sun whose approximate centre lies around $(l; b) \sim (240^\circ; -7^\circ)$, and that may be the progenitor of the Ring (see also Dinescu et al. 2005; Penarrubia et al. 2005). CMa was identified as a strong elliptical-shaped overdensity of M giants by the comparison of star counts in Northern and Southern Galactic hemispheres (from the Two Micron All-Sky Survey (2MASS); Cutri et al. 2003). The structure was suggested to be possibly associated with some globular (but see Penarrubia et al. 2005; Martinez-Delgado et al. 2005b) and open clusters (Crane et al. 2003; Bellazzini et al. 2004a; Paper I). The relic appears to have luminosity and size similar to the Sgr dSph (Paper I). The optical colour–magnitude diagram (CMD) we obtained in Bellazzini et al. (2004a, hereafter Paper II) revealed a narrow and well-defined main sequence (MS) typical of an intermediate-to-old (age ∼4–10 Gyr) and moderately metal deficient ($[M/H] \sim -0.5$) stellar system; these results have been fully confirmed by the deeper CMD presented by Martinez-Delgado et al. (2005a). A Blue Plume of possibly young stars or blue stragglers – also typical of dwarf spheroidal galaxies - has been detected in both optical CMDs. Carraro et al. (2005) detected the Blue Plume population in the background of several open clusters in the third Galactic quadrant. While these authors conclude that this population should be associated to the Norma and Perseus spiral arms of the Milky Way, it turns out that all the considered fields lie within the region of the sky where CMa is detected (from their table 1, $219^\circ \leqslant l \leqslant 254^\circ$; $-6.^\circ3 \leqslant b \leqslant +1.^\circ8$; see Paper I and Section 3), and in the same range of distances as CMa ($6.0 \leqslant D_\odot \leqslant 11.7$ kpc; see Paper I, Paper II and Section 4). Moreover, the Blue Plume populations studied by Carraro et al. (2005) appear to follow a distance–Galactic longitude trend quite similar to that found here for the red clump (RC) population of CMa (see Section 4.1.1).

The first results of a large spectroscopic survey provided an estimate of the systemic radial velocity and velocity dispersion of CMa ($V_r \simeq 110$ km s^{-1}, $\sigma = 13.0$ km s^{-1}; Martin et al. 2004b, hereafter Paper III), while an estimate of the systemic proper motion has been obtained by Momany et al. (2004). Martin et al. (2005, hereafter Paper IV) analysed the kinematics of more than 1400 red giant branch and RC stars around the centre of CMa, confirming the essence of the results of Paper III, namely that CMa stars have a systemic velocity and a velocity dispersion quite different from what was expected from Galactic disc stars at the considered distance and quite typical of Galactic dwarf satellite galaxies. Moreover, they detected a clear distance–radial velocity gradient among CMa stars that can be explained as the effect of on-going tidal disruption of the stellar system. A significant refinement of the proper motion estimate was also obtained in Paper IV. Finally, Dinescu et al. (2005) very recently obtained a new accurate estimate of the proper motion of CMa and concluded that (a) the system has a significant component of motion perpendicular to the Galactic plane ($W \simeq -50$ km s^{-1}) and (b) this W component of the space motion of CMa is in the opposite direction with respect to the expected W motion of stars associated with the Galactic warp. Other interesting investigations of the CMa relic, not strictly related to the present work or in a too preliminary stage to be fully useful for the analysis, can be found in Kinman, Saha & Pier (2004), Forbes, Strader & Brodie (2004), Sbordone et al. (2005) and Mateu et al. (2005).

Momany et al. (2004) suggested that the CMa overdensity may be an effect of the stellar component of the Galactic warp (Djorgovski & Sosin 1989; López-Corredoira et al. 2002; Yusifov 2004; Vig, Ghosh & Ojha 2005), whose broad southern maximum (as a south/north density asymmetry) lies in the range $240^\circ \leqslant l \leqslant 300^\circ$ (López-Corredoira et al. 2002; Vig et al. 2005). In Paper II and Paper III, in particular, we showed that such a conclusion can be reached only if the distance distribution of the adopted tracers (M giants) is neglected and that CMa is in fact an additional overdensity of different nature with respect to the large-scale warp of the Galactic disc. On the other hand, the disentanglement of the two structures may prove difficult, limiting our possibility to obtain a detailed global description of CMa and the warp (see Paper III for this discussion). A global analysis of CMa is also hampered by the large degree of contamination from Galactic stars, by the high and variable extinction towards the Galactic plane and by its proximity to us that imply a very low surface density in star counts per unit solid angle of sky (see Section 4.4).

It is clear that a large-scale study of CMa using a different tracer than the M giants used in the previous wide-field studies of the system would provide a very useful independent check of the results of Paper I and may help us to understand the relation between CMa and the warp. In Paper I, we showed that the RC of He-burning stars of the CMa system is clearly detected in the 2MASS data base, and in Paper II we used the RC stars to show that CMa is an independent structure, superposed on the Galactic warp. Here, we extend the use of RC stars to trace the whole structure of the outer Galactic disc, focusing on the CMa relic, and on the Galactic warp in its surroundings. In Section 2, we describe the adopted data set and assumptions, and we introduce our analysis method. In Section 3, we study the spatial distribution of overdensities rising from asymmetries between the Southern and the Northern Galactic hemisphere, focusing on the relation between Canis Major and the Galactic warp. In Section 4, we derive some fundamental parameters of CMa as a stellar system, and, finally, in Section 5 we summarize and discuss the main results of these analyses.

2 RC STARS AS TRACERS OF OUTER DISC STRUCTURES

From the 2MASS Point Source Catalogue, we extracted the sources comprising $l = 40^\circ$ and 320°, having $-30^\circ \leqslant b \leqslant 30^\circ$. The selected range of longitude and latitude covers the largest part of the Galactic disc, avoiding only the surroundings of the Galactic Centre, where the stellar crowding and the interstellar extinction may prove too severe for a useful analysis in the present context. Stars were selected according to the quality of the photometry and to avoid spurious and contaminated sources as in Bellazzini et al. (2003b). Moreover, only those stars having photometric uncertainties <0.3 mag both in *J and* in *K* magnitude have been included in the sample. The magnitudes of all the stars were corrected for extinction using the colour excesses interpolated on the *COBE*/Diffuse Infrared Background Experiment (DIRBE) maps (Schlegel, Finkbeiner & Davis 1998) and modified according to Bonifacio, Monai & Beers (2000), as done in Momany et al. (2004) and Paper III. Obviously, a 2D extinction map cannot account for the 3D distribution of the intersellar dust; thus the adopted correction may not always be good for nearby stars, but should be quite appropriate for the distant RC stars we

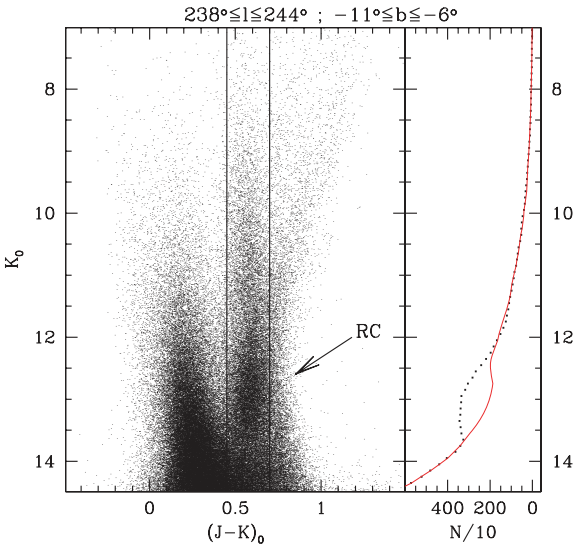

Figure 1. Left-hand panel: infrared CMD of a $6^\circ \times 5^\circ$ field near the centre of the CMa overdensity. The RC of CMa is indicated by the arrow. The vertical lines enclose the colour range in which we select candidate RC stars. Right-hand panel: LF of the selected RC stars (dotted black line). Note the strong bump associated with the RC of CMa at $K \sim 13.0$. The LF obtained exactly in the same way from the corresponding synthetic sample extracted from the R03 model (see Appendix A) is plotted as a red continuous line. The synthetic LF has been rescaled by a factor of 1/3 to match the total number of stars in the two samples.

are interested in. The extinction laws by Rieke & Lebofsky (1985) have been adopted. In the following, J, H and K magnitudes denote reddening-corrected magnitudes J_0, H_0 and K_0, unless otherwise stated. Only stars with $K < 15.0$ were retained for the analysis.

In Fig. 1, we show the $J-K$, K CMD of a low-extinction field near the centre of the CMa structure. The diagram is dominated by MS stars of the Galactic disc for $J-K \lesssim 0.5$; for $J-K \gtrsim 0.8$, the M giants are contributed by both the disc and the CMa, and the intermediate colour strip, $0.45 \leqslant J-K \leqslant 0.70$, enclosed by continuous lines in Fig. 1, should be dominated by RC stars located at various distances. While the M giant sequence of CMa can be revealed only with the subtraction of a control field symmetric with respect to the Galactic plane (Paper I), the RC of the system is clearly visible without subtraction in the range $12 \leqslant K \leqslant 14$ with an apparent peak around $K = 13$, as readily shown by the histogram in the left-hand panel of Fig. 1 (dotted black line), in excellent agreement with Paper I. Hence, RC stars are very promising tracers of the CMa structure. In the following discussion, we will limit our analysis to the stars in the colour strip enclosing the typical RC stars, $0.45 \leqslant J-K \leqslant 0.75$, as in Paper II (e.g. the region enclosed within parallel continuous lines in Fig. 1). In the left-hand panel of Fig. 1, we also plotted the luminosity function (LF) obtained with the same selection criteria from a synthetic sample of the same region of the sky extracted from the galaxy model by Robin et al. (2003, hereafter R03, red continuous line; see Appendix A for details). The R03 model includes a warped and flared disc (whose parameters have been fixed according to observations) and the effect of the displacement of the Sun with respect to the Galactic plane by 15–16 pc (towards the Galactic North; Hammersley et al. 1995, R03). It is interesting to note that the R03 model excellently reproduces the observed LF for $K < 12.3$ and $K > 13.7$, but completely lacks the strong bump around $K = 13$ that we attribute to the RC of Canis Major.

With respect to M giants, RC stars may suffer from a larger degree of contamination by unrelated sources. While for $J-K \geqslant 1.0$ the only possible contaminants for M giants are M dwarfs at faint magnitudes ($K \geqslant 12.0$), our colour-selected RC sample may be contaminated by K giants essentially at any magnitude, and significant numbers of both M and G dwarfs can be pushed into the RC colour range by photometric errors for $K > 14.0$ [see López-Corredoira et al. 2002, (hereafter LO2) and Appendix A for discussion]. However, all the results presented below are in the form of subtractions of star counts in the Southern and Northern Galactic hemispheres. Since the degree of contamination from Galactic sources as a function of magnitude should be similar in both hemispheres, the subtraction should minimize any spurious effect associated with contaminants (see Appendix A). Moreover, all the results presented below remain unaltered if we limit our sample to RC stars having $K \leqslant 14.0$, where the contamination by dwarfs is not overwhelming (López-Corredoira et al. 2002). In Appendix A, we study the problem of contamination by dwarfs in some detail, showing that (a) in spite of the large fraction of dwarf that may contaminate our samples and of the presence of north–south (NS) differences in the degree of contamination, the adopted technique traces trustworthy real asymmetries in the density of distant giants, for $K \leqslant 14.0$ and (b) the intrinsic asymmetry due to the $\simeq$15 pc displacement of the Sun above the Galactic plane (Hammersley et al. 1995) has a negligible effect on our analysis.

On the other hand, RC stars should be intrinsically more numerous than M giants, and they provide a completely independent and more reliable distance scale compared with the photometric parallax of M giants [see Bellazzini et al. (2003b), Majewski et al. (2003), Paper I, Paper II and Paper III].

If not stated otherwise, we will use in the following analysis only stars with $|b| > 5\overset{\circ}{.}0$ to avoid the regions where the extinction is most severe. Fig. 2 shows that once the $|b| > 5\overset{\circ}{.}0$ strip is excluded, the region considered in the present analysis is largely free from high-extinction regions (e.g. where $A_K > 0.3$ mag). Since most of the structures we are interested in are enclosed in the latitude strip $|b| \leqslant 15\overset{\circ}{.}0$, most of the following analysis is limited to this range. Note that the 2MASS Point Source Catalogue is complete down to

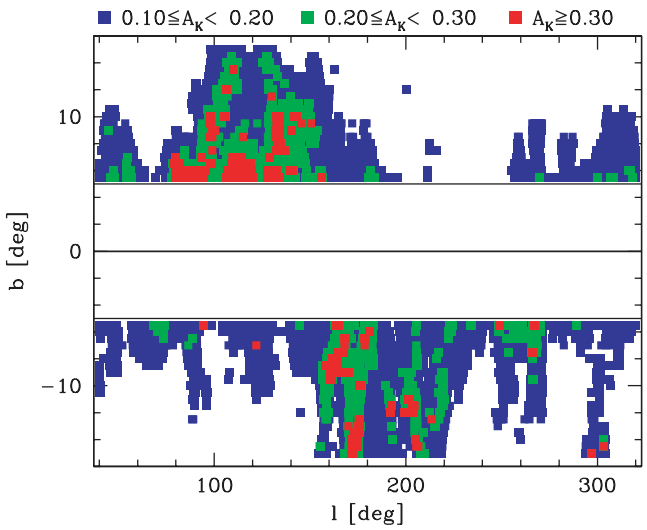

Figure 2. Map of the extinction (in K band) for the range of Galactic longitude and latitude considered in the present analysis. The *COBE*-DIRBE reddening maps (Schlegel et al. 1998) have been interpolated on a grid whose knots are spaced by $0\overset{\circ}{.}5$ both in l and in b.

$K_S = 14.3$ (Cutri et al. 2003); hence the luminosity range in which most of the RC stars we will consider lies ($11.0 \lesssim K \lesssim 14.0$) is not expected to suffer from problems of incompleteness.

2.1 CMa and the warp as south–north overdensities

It has to be noted that the origin of disc warps and the relationship between gaseous and stellar warps are far from understood (Binney 1992; Kuijken & Garcia-Ruiz 2001). Moreover, the characterization of the stellar warp of the Milky Way is quite poor and uncertain mainly because of the problems inherent with the analysis of stellar fields at low Galactic latitudes. Finally, it is important to realize that the adopted parametrization may describe different characteristics of the warp and may induce some confusion in the use of terms. For instance, Djorgovski & Sosin (1989) identified the stellar warp as a sinusoidal variation of the mean latitude of their tracers (namely *IRAS* sources) as a function of longitude. In this case, the 'maximum of the warp' coincides with the maximum *angular height* above the Galactic equator, similar to the parametrization adopted when dealing with the gaseous warp. On the other hand, L02 described the warp as the sinusoidal variation of the ratio of star counts in Northern and Southern Galactic hemisphere as a function of longitude, hence their 'maximum of the warp' is the region where the Southern (or Northern) projected overdensity reaches its maximum. The two definitions may provide very different views, depending on the structure of the disc and on the relative 3D positions of the observed structures and the Sun. Since the CMa galaxy was identified as a south/north overdensity, it should be compared with the warp as a south/north overdensity (López-Corredoira et al. 2002), since this is the only relevant parameter in this context. The parametrization of the amplitude of the warp as the artificial shift to apply to the Galactic plane to match the star counts in the Northern and Southern hemisphere (as done by Momany et al. 2004) is not a fair description of south/north overdensities in the present context, since it turns into a comparison of stars lying at different distances, as shown in Paper III. Hence, in the following we will always deal with CMa and the warp as South/North overdensities.

2.2 The construction of subtracted density maps

Most of the following analysis will make use of subtracted density maps obtained form the above-described sample of colour-selected RC stars. In this section, we will describe in detail how these maps are obtained.

RC stars are widely used as distance indicators (see e.g. Paczynski & Stanek 1998; López-Corredoira et al. 2002; Sarajedini et al. 2002; Babusiaux & Gilmore 2005, and references therein). In Paper II, we assumed $M_K = -1.5 \pm 0.2$ for the RC of CMa, since, according to the theoretical models by Salaris & Girardi (2002), this interval encloses the absolute K magnitude of the RC for populations of metallicity $-0.4 \lesssim [M/H] \lesssim -0.7$ and age between 4 and 10 Gyr, i.e. the proper age and metallicity for CMa (see Paper II). Here, we adopt the same assumption to obtain the distance of each RC star in our sample. These individual distances should be regarded with some caution since the adopted distance scale is optimized for the RC of CMa and may provide misleading answers when applied (a) to contaminant sources that are not RC stars (see Section 2) and (b) to RC stars outside the age and metallicity ranges outlined above. On the other hand, the range of age and metallicity of stellar populations in the outer Galactic disc that produces RC stars should not be too different from that outlined above. Hence, the assumed global distance scale is expected to provide a reasonable description of the overall spatial distribution of RC stars in this region of the Galaxy and a reliable representation of the CMa system. In particular, it should be considered that RC stars are much less sensitive to metallicity and age variations in the considered populations compared to M giants (see, Crane et al. 2003; Majewski et al. 2003; Rocha-Pinto et al. 2005, Paper I and references therein). Finally, it should also be recalled that in the following we will deal only with *subtracted* density distributions: the subtraction should cancel out many of the above effects if, as it is very reasonable to assume, at a given Galactocentric distance the age and metallicity distributions are similar in both Galactic hemispheres.

We used the distances of individual RC stars in our sample to obtain their Cartesian heliocentric coordinates

$$x = \mathrm{D}_\odot \cos(l)\cos(b)\,[\mathrm{kpc}] \quad (1)$$

$$y = \mathrm{D}_\odot \sin(l)\cos(b)\,[\mathrm{kpc}] \quad (2)$$

$$z = \mathrm{D}_\odot \sin(b)\,[\mathrm{kpc}]. \quad (3)$$

In this system, the coordinates of the Sun are $(x, y, z) = (0.0, 0.0, 0.0)$ kpc, and the centre of the Galaxy is located at $(x, y, z) = (+8.0, 0.0, 0.0)$ kpc, having assumed that the distance to the Galactic Centre is 8.0 kpc. To avoid any possible effect of local inhomogeneities in the vicinity of the Galactic plane, we also removed the stars having $|z| < 0.5$ kpc. Given the adopted selections, this is equivalent to excluding stars within $\simeq$1kpc from the Sun.

From these samples, we computed the density of RC stars on an x, y grid with boxes of size 1×1 kpc, spaced by 0.5 kpc both in x and in y. The overlapping between adjacent boxes ensures some degree of smoothing, providing more clearly readable maps. In this way, we obtained x, y density maps of the Southern and Northern hemisphere that can be subtracted, 'pixel to pixel', to obtain a map of the residual surface density in the x,y plane, that is residual maps of the Galactic plane as seen from the Galactic pole. The density at each point of the subtracted map is computed as

$$\rho_{(x,y)} = \left[n^{\mathrm{South}}_{(x,y)} - n^{\mathrm{North}}_{(x,y)}\right].$$

Note that $n^{\mathrm{South}}_{(x,y)}$ and $n^{\mathrm{North}}_{(x,y)}$ are a sort of 'column' density, since at the position $(x_0;y_0)$ the derived density is equal to the number of RC stars having $x_0 - 0.5 \leqslant x \leqslant x_0 + 0.5$ and $y_0 - 0.5 \leqslant y \leqslant y_0 + 0.5$, *at any* z within the limits of our sample. The imposed selection in latitude ($5\overset{\circ}{.}0 < |b| \leqslant 15\overset{\circ}{.}0$) implies that the range in z sampled by different pixels of the grid varies with their heliocentric distance. In particular, at $\mathrm{D}_\odot = 5.0$ kpc the sampled range of z is $0.5 \lesssim |z| \lesssim 1.5$ kpc, at $\mathrm{D}_\odot = 10.0$ kpc: $0.9 \lesssim |z| \lesssim 2.6$ kpc, at $\mathrm{D}_\odot = 13.0$ kpc: $1.1 \lesssim |z| \lesssim 3.3$ kpc. It is important to realize that this has no consequence for the subtracted densities $\rho_{(x,y)}$, since each pair of pixels to be subtracted has exactly *the same volume*.

Since a large absolute density residual (e.g. in number) does not necessarily imply a statistically significant signal, it is mandatory to obtain the subtracted density maps also in terms of signal-to-noise ratio, that is in units of σ:

$$\rho_{(x,y)} = \left[n^{\mathrm{South}}_{(x,y)} - n^{\mathrm{North}}_{(x,y)}\right] \Big/ \sigma_{(x,y)}$$

where

$$\sigma_{(x,y)} = \sqrt{n^{\mathrm{South}}_{(x,y)} + n^{\mathrm{North}}_{(x,y)}}.$$

Subtracted maps in terms of number density provide a physical idea of the extent of the detected overdensities, while subtracted maps in σ units allow us to discriminate structures that are statistically reliable and significant from those that can arise from mere statistical fluctuations.

3 OVERDENSITIES IN THE OUTER DISC

Fig. 3 shows the maps of residuals obtained by subtracting the Northern hemisphere density map from the Southern hemisphere density map in terms of number density (panel a) and in units of σ (panel b). We recall here that the regions $0^\circ \leqslant l \leqslant 40^\circ$ and $320^\circ \leqslant l \leqslant 360^\circ$ are excluded from the present analysis. In Appendix A, it is shown that while the effect of contamination by dwarfs should not significantly affect subtracted density maps for $K \leqslant 14.0$, it may become quite relevant at fainter mag. In this section, we present subtracted maps that also include stars having $14.0 < K < 15.0$ to avoid abrupt distance thresholds in the proximity of the regions of interest. We caution the reader that the reliability of the maps may be drastically reduced beyond the heliocentric circle corresponding to the $K = 14.0$ limit that is always clearly shown in Figs. 3–5, as a reference. According to the results of Appendix A, the contamination by dwarfs can seriously affect the maps also around $l = 180^\circ$. On the other hand, the main structures we deal with in the following analysis lie safely in the range of latitudes and distances that should be correctly probed by our subtracted-density technique (see Appendix A).

With the only exception of a few limited low-significance structures near the edges of the map (in particular near $l = 40^\circ$, probably due to edge effects), the strongest south–north (SN) overdensities are confined in the third and fourth Galactic quadrants ($180^\circ \leqslant l \leqslant 360$). This is not unexpected since it is well known that the Galactic disc is warped towards the South Galactic hemisphere for $180^\circ \leqslant l \leqslant 360$ and towards the North Galactic hemisphere for $0^\circ \leqslant l \leqslant 180$ (Djorgovski & Sosin 1989; López-Corredoira et al. 2002; Yusifov 2004; Vig et al. 2005, and references therein). The third and fourth Galactic quadrants appear to be dominated by a wide, galactic-scale overdensity that extends over the whole half of the disc with $l > 180^\circ$. On top of this large-scale asymmetry, there is a strong and spatially confined overdensity, with an elongated, approximately elliptical shape, with a denser roundish core located at $(x, y) = (-3.7, -6.4$ kpc), towards $l = 240^\circ$, at $R_{\rm GC} \sim 13.0$ kpc and $\mathrm{D}_\odot \sim 7.5$ kpc. This is the Canis Major structure, as described in Paper I, Paper II and Paper III. Note that a secondary core that appears towards $l \simeq 280^\circ$ in Fig. 3(a) is revealed as a non-statistically significant structure by the inspection of the map in σ units [Fig. 3(b)].

The linear 'finger of God' structures between $l \sim 200^\circ$ and $\sim 220^\circ$, and at $l \sim 250^\circ$ correspond to asymmetric features in the distribution of the extinction (see Fig. 2) and are likely artefacts associated with the (unknown) 3D distribution of the interstellar dust. These features are present in all the SN maps presented in this paper and will not be discussed further. Also note that the strongest and most significant parts of the detected overdensities (including the body of CMa) lie within the circle enclosing the RC stars with $K \leqslant 14.0$ (inner heliocentric long-dashed circle, at $\mathrm{D}_\odot = 12.6$ kpc), that is in the region where the contamination by dwarf stars is less severe [i.e., the contribution of dwarfs is less than 50 per cent, according to López-Corredoira et al. 2002 and the contribution of dwarfs to subtracted densities is lower than 30 per cent; see Appendix A].

Fig. 4 shows the maps of residuals obtained by subtracting the Southern hemisphere density map from the Northern hemisphere density map, in terms of number density (panel a) and in units of σ (panel b). Also, in this case the detected overdensities are confined to the Galactic quadrants that are expected to host the northern lobe of the warp. The observed asymmetry has a large scale – as in the SN maps – but is weaker and less significant than the large-scale Southern asymmetry. This may be due to differences

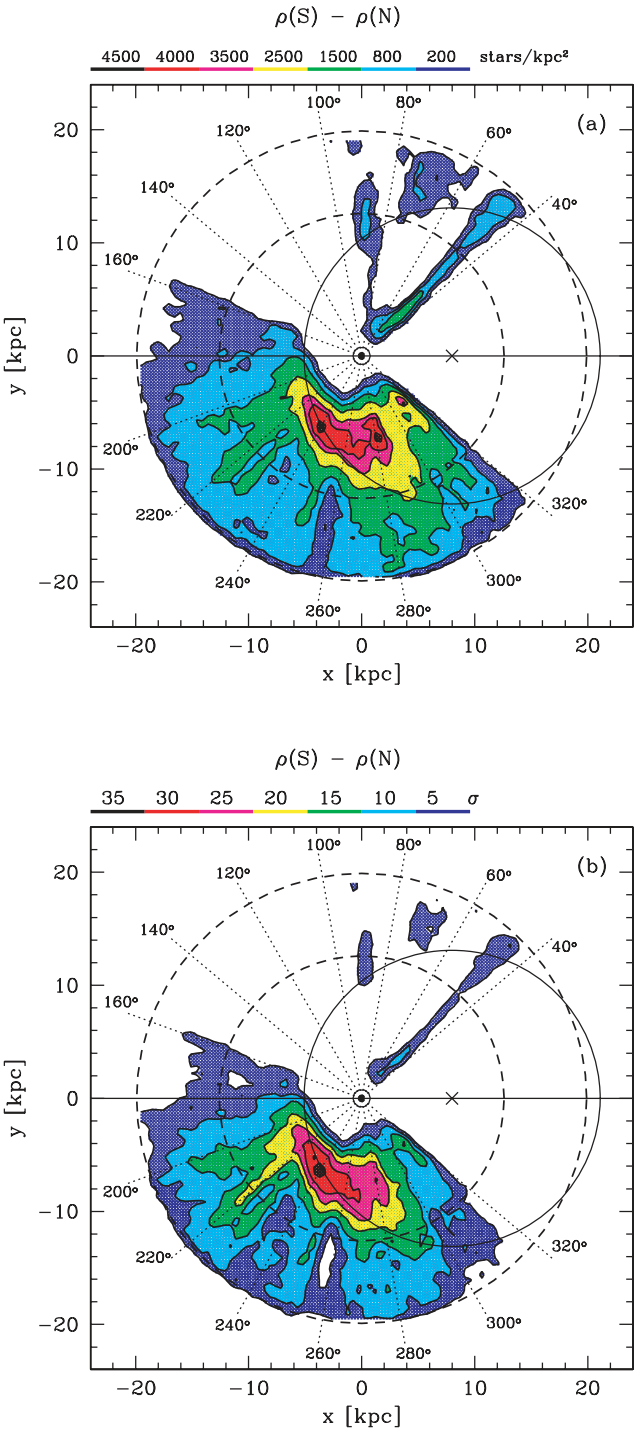

Figure 3. Subtracted density maps (SN) in terms of number density (panel a) and in units of σ (signal-to-noise ratio; panel b). The direction of Galactic longitudes from $l = 40^\circ$ to 320°, with steps of 20°, are indicated as labelled dotted lines. The encircled dot marks the position of the Sun, the $\times$ symbol indicates the Galactic Centre. Long-dashed circles are centred on the Sun: the outer circle indicates the distance limit of our analysis, corresponding to RC stars having $K = 15.0$, the inner circle encloses the region sampled by RC stars having $K \leqslant 14.0$, i.e. the range in which the contamination by dwarfs should be moderate. The continuous circle is centred on the Galactic Centre and has a radius $R_{\rm GC} = 13.1$ kpc, corresponding to the heliocentric distance of $\mathrm{D}_\odot = 7.2$ kpc for the centre of the Canis Major structure at $l = 240^\circ$ (Paper III). The region within $\pm 40^\circ$ in longitude from the Galactic Centre is excluded from the present analysis.

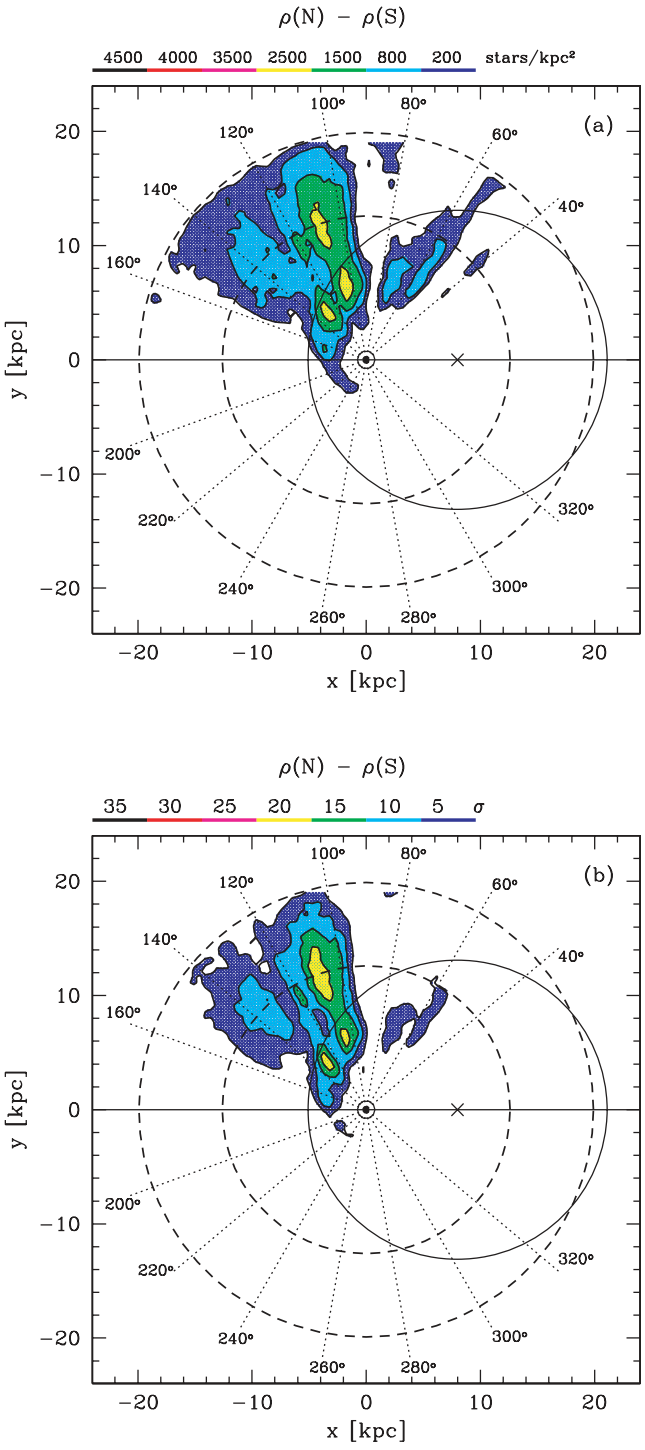

Figure 4. Subtracted density maps (NS) in terms of number density (panel a) and in units of σ (signal-to-noise ratio; panel b). The symbols are the same as in Fig. 3.

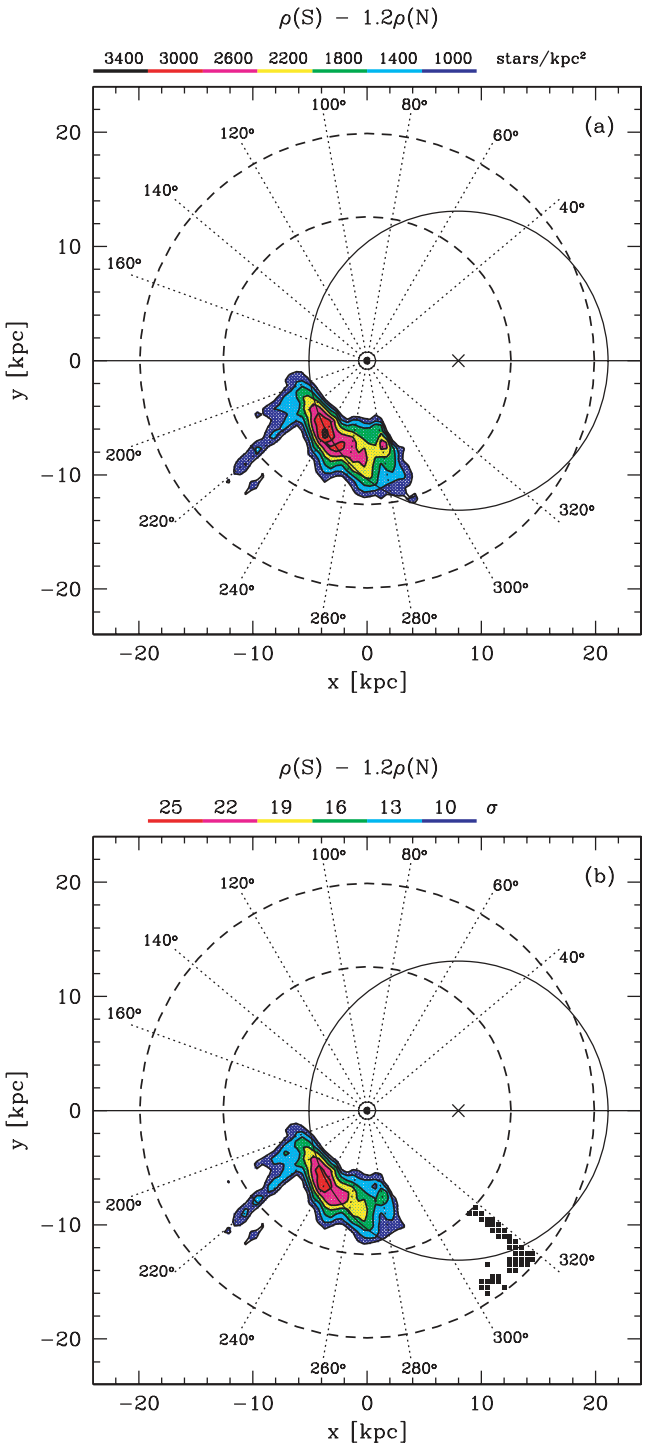

Figure 5. Subtracted density maps (SN) in terms of number density (panel a) and in units of σ (panel b). In this case, the densities in the Northern hemisphere maps have been rescaled by a factor of $\times 1.2$ to attempt to remove the large-scale asymmetry that we identify as due to the Galactic warp. In panel (b), we reported as small filled squares the pixels of the map where *negative* residuals larger than 10σ are detected. All the other symbols are the same as in Fig. 3.

in the structure of the Northern and the Southern warp (see e.g. Porcel, Battaner & Jiménez-Vicente 1997; Yusifov 2004) and to the effect of the displacement of the Sun with respect to the Galactic plane (Hammersley et al. 1995). However, in the present context it is interesting to note that (a) there is no overdensity comparable to CMa in the Northern hemisphere and (b) the most significant asymmetries lie in the range $100^\circ \leqslant l \leqslant 140^\circ$, that is at $\sim 180^\circ$ from the densest part of the large-scale Southern overdensity ($280^\circ \leqslant l \leqslant 320^\circ$).

The inspection of Figs 3 and 4 clearly demonstrates that CMa is the strongest (35σ) overdensity of the whole Galactic disc.

Moreover, it is strongly spatially confined (the two innermost density contours have a typical scale of ∼4 × 2 kpc) and there is no corresponding structure either on the opposite side of the disc ($l \sim 60^\circ$) or at the reflected position about the y- or x-axis.

Note that the detected excess of RC stars is quantitatively very similar to what was found for M giants in Paper I (in terms of σ and of fractional excess). CMa appears as a strongly concentrated, cored overdensity on top of a galactic-scale asymmetry that has all the characteristics of the Galactic warp.

3.1 Removing the large-scale asymmetry

If the global smooth overdensity is related to the Galactic disc (i.e. it reflects the warp asymmetry), it should be possible to subtract it from the maps of Fig. 3. Since the overall number of southern RC stars in our sample is 1.2 times that found in the Northern hemisphere, as the simplest assumption we rescale the density of the Northern map by this factor and repeat the subtraction. The adopted normalization should also account for the effect of the off-plane position of the Sun. The resulting maps of residuals are shown in Fig. 5, in terms of both number density (panel a) and σ units (panel b). Adopting a safe 10σ cut, the only surviving structure is CMa plus tiny traces of the already-discussed finger-of-God features at $l \sim 220^\circ$.

Note that large negative residuals ($\geqslant 10\sigma$) appear only near the edges of the maps [Fig. 5(b)]. This means that the rescaled northern density map is a reasonable model of the large-scale overdensity observed in the Southern hemisphere. We tried different simple models fitting the observed overall decline of the large-scale overdensity with $R_{\rm GC}$: in all cases the only overdensity surviving the subtraction of the model from the southern density map is CMa, in all cases displaying the characteristic shape shown in Figs 5(a) and (b). This exercise strongly supports our interpretation of the southern overdensities in the considered region of the Galaxy in terms of a large-scale Galactic asymmetry (warp) plus an additional unexpected elongated compact structure with a dense core, i.e. the Canis Major overdensity.

3.2 Comparison with a warp model

In response to the suggestion that the CMa overdensity may be associated with the Galactic warp, we have compared the observed characteristics of CMa with two different models of the Galactic warp, namely that enclosed in the Galactic model by R03, in Paper II, and the warp model by Yusifov (2004), in Paper III. In both the cases, we found that the models were clearly unable to reproduce the very compact structure of CMa. In particular, the distance profile of the overdensities predicted by models is much more extended than what is observed for Canis Major. Here, we extend the comparison to the model by L02 that has been constructed to fit the overall distribution of RC stars in the Galactic disc.

In order to compare density distributions obtained with the same technique, we constructed a Monte Carlo realization of the L02 model, and we applied the same selections as to the observed sample (i.e. $5^\circ \leqslant |b| \leqslant 15^\circ$ and $|z| \geqslant 0.5$ kpc). We extended the L02 model outside its maximum Galactocentric distance ($R_{\rm GC} = 13.0$ kpc) with the following assumptions for the average elevation of the disc above the plane z_w (see equation 20 in L02):

$$z_w = C_W R\,[\mathrm{kpc}]^{5.25} \sin(\Phi - \Phi_W) + 15.0$$

for 13.0 kpc $< R_{\rm GC} \leqslant$ 16.0 kpc, where $C_W = 0.0012$, $\Phi_W = -5.^\circ 0$ and

$$z_w = 0.0$$

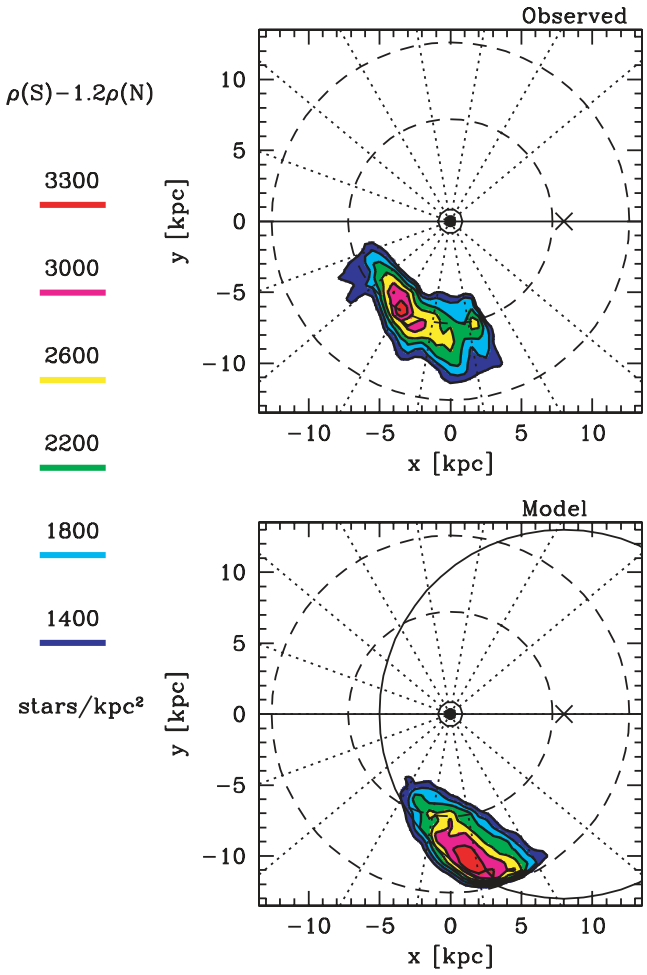

Figure 6. Subtracted density maps (SN) from the observed sample (upper panel) and from the López-Corredoira et al. (2002) model (lower panel). The model map has been normalized to have the same maximum density as the observed one. The inner long-dashed circle has a radius $r = \mathrm{D}_\odot = 7.2$ kpc, i.e. the heliocentric distance of CMa (Paper III). The outer long-dashed circles enclose the region populated by RC stars having $K \leqslant 14.0$. Both samples have also been limited to $R_{\rm GC} < 17.0$ kpc. The continuous-line galactocentric circle plotted in the lower panel of the figure, having radius =13.0 kpc, shows that the relevant comparison is performed inside the extrapolation region, hence the adopted form of the extrapolation cannot affect our results. Black dots in the lower panel indicate negative residuals larger than 50 per cent, corresponding to the northern lobe of the warp.

for $R_{\rm GC} > 16.0$ kpc. This extrapolation produces a regime of nearly constant elevation for 13.0 $< R_{\rm GC} \leqslant$ 16.0 kpc and a drop to the plane at larger galactocentric distances that appear as the most appropriate for the Southern warp, according to Porcel et al. (1997) and Yusifov (2004), for example. For homogeneity, we applied the $R_{\rm GC} = 17.0$ kpc cut also to the observed sample. Note, however, that the region relevant for the comparison is largely included within the $R_{\rm GC} = 13.0$ kpc limits, hence the adopted extension of the L02 model must have little effect on our results (see Fig. 6).

Finally, we limit the comparison to stars within $\mathrm{D}_\odot = 12.6$ kpc, corresponding to the $K \leqslant 14.0$ for RC stars. After applying all of the above selection criteria, the Monte Carlo realization of the L02 model contains 10^6 particles. Considering these particles as the analogues of RC stars, we have obtained subtracted density maps from the model in exactly the same way as we did for real stars (see

Section 2.2). We normalized the density scale of the model map by requiring that the maximum density is the same in the synthetic and observed map. We have also tried several other normalizations and found that the essence of the results remains unchanged.

In Fig. 6, the observed SN subtracted map (upper panel) is compared to the same map obtained from the L02 model. Both maps are represented in the same scale of density excess. The differences between the two maps are clearly evident. In the model map, the warp appears as a large wedge-shaped overdensity, somewhat similar – in shape – to the densest part of the large-scale overdensity observed in Fig. 3. The density of this feature reaches a broad maximum in the range $270^\circ \leqslant l \leqslant 280^\circ$, over a large range of heliocentric distances, around $(x, y)_{[\mathrm{kpc}]} \simeq (1.5; -10.3)$ – while the maximum of the observed density occurs at $l \simeq 240^\circ$ and $(x, y)_{[\mathrm{kpc}]} \simeq (-3.5; -6.2)$, more than 6 kpc apart. It is quite clear that the model is totally unable to reproduce the CMa structure presented in the upper panel of Fig. 6 as the only significant overdensity, extending from $l \sim 200^\circ$ to $\sim 275^\circ$, with its compact elliptical shape and short minor axis, and with its core at $l = 240^\circ$. The differences between the two structures (CMa and the L02 warp model) clearly suggest that they are of a different nature and cannot be identified with one another, confirming the results presented in Paper II and Paper III (see also Fig. 1).

Despite the large differences shown in Fig. 6, it may still be argued that the L02 warp model still predicts some SN overdensity at the position of CMa. Are the observed and predicted distributions *locally* similar at this position? To test this possibility, we recur to the optical CMD of the *XMM* field (F-*XMM*, at $l = 244\overset{\circ}{.}2$ and $b = -8\overset{\circ}{.}2$) we presented in Paper II, that is reproduced in the middle panel of Fig. 7. To have an idea of how the CMD of an ensemble of old stars distributed according to the L02 model would appear, we proceeded as follows. (1) We take as template population the photometry of $\sim$130 000 stars of the globular cluster 47 Tucanae presented by Bellazzini et al. (2004b). (2) We extracted, at random, 20 000 stars from this sample and we corrected their magnitude for extinction and for distance [assuming $E(B-V) = 0.04$ and $(m-M)_0 = 13.29$ for the cluster, from Ferraro et al. (1999)]. (3) We assigned to each star a distance randomly extracted from the distance distribution predicted by the L02 model towards $(l, b) = (244\overset{\circ}{.}2, -8\overset{\circ}{.}2)$. (4) We corrected for the corresponding distance moduli and for the reddening of the *XMM* field [$E(B-V) = 0.14$, see Paper II].

The *synthetic* CMD thus obtained is shown in the upper panel of Fig. 7. Its morphology is completely different from that of the observed diagram. Stars around the turn-off (TO) point of the cluster form a vertical sequence from $V \sim 17.0$ to $V \sim 20.0$ that abruptly bends to the red for $V > 20.0$ in the way typical of CMDs of Galactic fields that sample populations at widely different distances along the LOS. This result is similar to what we obtained in Paper II while comparing the F-*XMM* CMD with the predictions of the warped and flared Galactic model by R03. Note that $\sim$30 per cent of the stars plotted in the upper panel of Fig. 7 have associated distances that place them in the regime in which we adopt an extrapolation of the L02 model. However, repeating the experiment while forcing the selection of stars with $R_{\mathrm{GC}} \leqslant 13.0$ leads to a CMD having a morphology essentially indistinguishable from that shown here. Hence, also in this case, the adopted extrapolation of the L02 model has a negligible effect on our results. In contrast, the F-*XMM* CMD shows a clear and narrow MS that bends continuously from the TO (around $V \sim 18.5$) to the limit of the survey, clearly resembling a bound stellar system. This similarity is made clearer by the comparison with the CMD shown in the lower panel of Fig. 7. This synthetic diagram

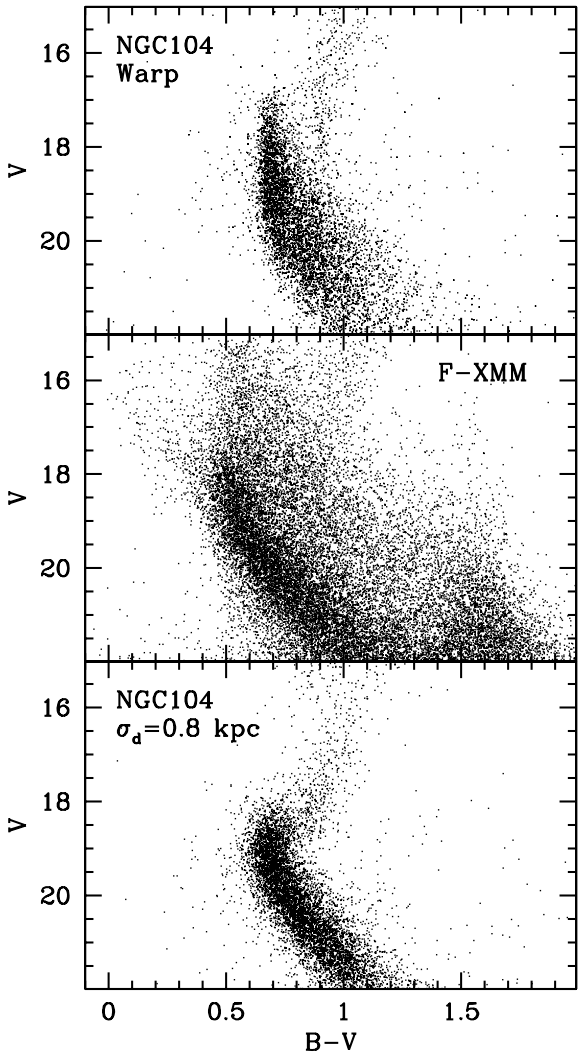

Figure 7. Synthetic (upper and lower panels) and observed (middle panel) CMDs towards $(l; b) = (244\overset{\circ}{.}2; -8\overset{\circ}{.}2)$. Upper panel: CMD of $\sim$20 000 stars randomly extracted from the photometry of the cluster 47 Tucanae by Bellazzini et al. (2004b), as it would appear if the considered stars were distributed according to the distance distribution predicted by the Lopez-Corredoira at al. warp model in the above direction. Middle panel: observed CMD towards $(l; b) = (244\overset{\circ}{.}2; -8\overset{\circ}{.}2)$ (*XMM* field; from Paper II). Lower panel: CMD of $\sim$20 000 stars randomly extracted from the photometry of the cluster 47 Tucanae by Bellazzini et al. (2004b), as it would appear if the considered stars were distributed according to a Gaussian distribution having mean $\mathrm{D}_\odot = 7.2$ kpc and standard deviation $\sigma = 0.8$ kpc, i.e. the LOS distance distribution of CMa as estimated by Martinez-Delgado et al. (2005a).

has been obtained repeating steps 1, 2 and 4 described above but assigning to stars distances extracted from a Gaussian distribution having a mean $\mathrm{D}_\odot = 7.2$ kpc (i.e. the distance of CMa as derived in Paper III) and $\sigma = 0.8$ kpc, as derived by Martinez-Delgado et al. (2005a) for CMa. Except for the foreground field population that is, obviously, present in the F-*XMM* and absent in the higher latitude 47 Tuc field, the two MS features are strikingly similar. This test confirms that the observed CMa overdensity in not predicted by current models of the Galactic warp, neither on global nor on local scales. While all the considered models predict that the Galactic warp should provide some overdensity at the position of CMa, in good agreement with the results shown in Fig. 3, none of them is able

to reproduce anything remotely similar to the extremely compact, cored structure we observe in Canis Major.

It should be recalled that the Galaxy models including a warped and flared outer disc, as those considered here and in Paper II and Paper III, are not meant to provide a perfect representation of the Galaxy, in particular for what concerns the outer parts of the Galactic disc where the available observations are scanty and uncertain over large ranges of longitude. Hence, the fact that these models are unable to reproduce the observed structure of CMa is not an ultimate proof that Canis Major cannot be a substructure of the Galactic disc. On the other hand, this is a proof that (a) Canis Major is a truly unexpected structure, since no similarly spatially confined and dense structure is included in existing warped and flared models of Galactic disc and, (b) the CMa structure is fairly different from the general expectations of an overdensity due to the Galactic warp, since it is a compact elongated and cored structure instead of a large wedge-shaped lobe, as shown in Fig. 6, and, above all, it appears at a significantly different position.

3.2.1 *The Argo structure*

While the present paper was near completion, a preprint was posted (Rocha-Pinto et al. 2005, hereafter RP05) studying the distribution of 2MASS M giants at low galactic latitudes ($|b| \leqslant 20^\circ$). Adopting an extinction grid with a finer resolution compared to previous analyses of M giants (Crane et al. 2003; Majewski et al. 2003, Paper I) and using a star counts model to subtract the smooth Galactic components, they were able to follow overdensities down to lower absolute latitudes ($|b|$) than, for instance, Paper I. They found that, in the $220^\circ \leqslant l \leqslant 320^\circ$ region, all the existing overdensities are enclosed in the range of heliocentric distances 6.0 kpc $< D_\odot <$ 20 kpc. They confirm the presence of the CMa overdensity in this range, but they claim that it is part of a larger and denser structure, centred around $l \simeq 290^\circ$, that they interpret as a large dwarf galaxy which they name *Argo*. They suggest that Argo and CMa can be erroneously seen as separated entities only because of a plume of extinction located at $l \simeq 265^\circ$ extending to $b \simeq -12^\circ$ (see Figs 2 and 8) that introduces an artificial discontinuity in the surface density.

In Fig. 8, we present the SN subtracted surface density map of RC stars in the range $200^\circ \leqslant l \leqslant 320^\circ$, obtained by counting stars (in the distance range $5.0 \lesssim D_\odot \lesssim 13.0$ kpc) within $4^\circ \times 4^\circ$ boxes spaced by 2° both in longitude and in latitude. In this case also, stars with $|b| < 5.^\circ 0$ have been included in the sample for a better comparison with RP05. The main body of the claimed Argo structure is clearly traced, in surface density, also by RC stars. In Fig. 8, it appears as a strong, elongated overdensity with a broad maximum around $l \sim 290^\circ$–310°, with CMa placed at its low-longitude edge (compare with figs 1 and 3 of RP05).

The maps displayed in Figs 3(a) and (b) (as well as Figs 5–7) show that *there is no spatially confined 3D structure* corresponding to this strong *surface* overdensity. Integrating over the range 6.0 $< D_\odot <$ 20 kpc along the $l \sim 280^\circ$–300° direction implies summing up the contribution of all the stars encountered along the LOS that crosses the maximum of the overdensity produced by the Galactic warp. In any case, while in terms of surface density – integrated over 14 kpc along the LOS – CMa is a much weaker structure compared to Argo (see Fig. 8), it corresponds to a much more *spatially confined* structure: CMa spans the range $5 \lesssim D_\odot \lesssim 12$ kpc, with a LOS HWHM of just ∼2.0 kpc (see Paper II, Martinez-Delgado et al. (2005a) and Section 4.1). The major axis of CMa is approximately oriented along the path of a nearly circular orbit around the centre

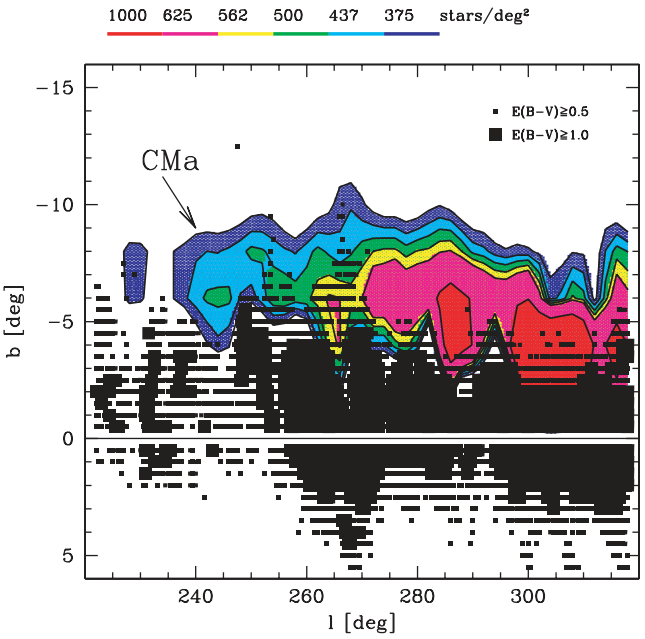

Figure 8. Subtracted map (SN) in terms of surface density in the sky for RC stars in the range $11.5 \leqslant K \leqslant 14.0$. The surface density has been computed on a grid of $4^\circ \times 4^\circ$ pixels spaced by 2° both in latitude and in longitude. In this case, stars with $|b| < 5.^\circ 0$ have also been included in the sample. The position of CMa is indicated by a labelled arrow. Small squares mark positions where the reddening is $0.5 \leqslant E(B-V) < 1.0$, large squares correspond to reddening in excess of 1.0 mag.

of the Galaxy (see Figs 5 and 11), consistent with the *N*-body simulation presented in Paper IV (see Section 4.2). On the other hand, the Argo structure corresponds to a part of the large-scale southern overdensity that spans more than 15 kpc in heliocentric distance, towards $l \sim 290^\circ$, and it does not appear as a coherent, cored structure as CMa (see Fig. 3).

The above arguments are clearly displayed in Fig. 9, where we consider the surface density of RC stars confined to the very narrow range of Galactocentric distances including most of the main body of CMa ($12.0 \leqslant R_{GC} \leqslant 14.0$ kpc). The subtracted surface density map in the upper panel of Fig. 9 has been obtained in the same way as Fig. 8, but is expressed in terms of fractional density excess to allow a comparison with the L02 model. It is quite evident that at this spatial location the only strong overdensity is CMa, while Argo has completely disappeared. On the other hand, the fractional excess due to the warp (integrated over $5^\circ \leqslant |b| \leqslant 15^\circ$, Fig. 9, lower panel), as predicted by the L02 model, reaches its maximum at the longitude corresponding to the maximum density of Argo ($l \sim 290^\circ$–300°).

There is also a quantitative self-consistency problem to consider. RP05 derive (from M giants) an estimate of the total luminosity of $L = 3.7$–$15 \times 10^6\,L_\odot$ for Argo. Limiting ourselves to the stars contributing to the map of Fig. 8 and within $265^\circ \leqslant l \leqslant 320^\circ$, we count an excess of more than 1.8×10^6 RC stars. With the assumptions stated in Section 4.3, we obtain a total luminosity of $L \sim 1.2 \times 10^9$, orders of magnitude larger than the R05 estimate. Note that our estimate should be considered as a lower limit since (a) the contribution of CMa is not included, while RP05 consider it as a part of Argo, and (b) we limited the calculation to the approximate distance range $5 \leqslant D_\odot \leqslant 13$ kpc, while R05 integrate over 6.0 $< D_\odot <$ 20 kpc. Hence, the beautiful consistency among the luminosity estimates obtained from M giants, RC stars and MS stars achieved for CMa (see

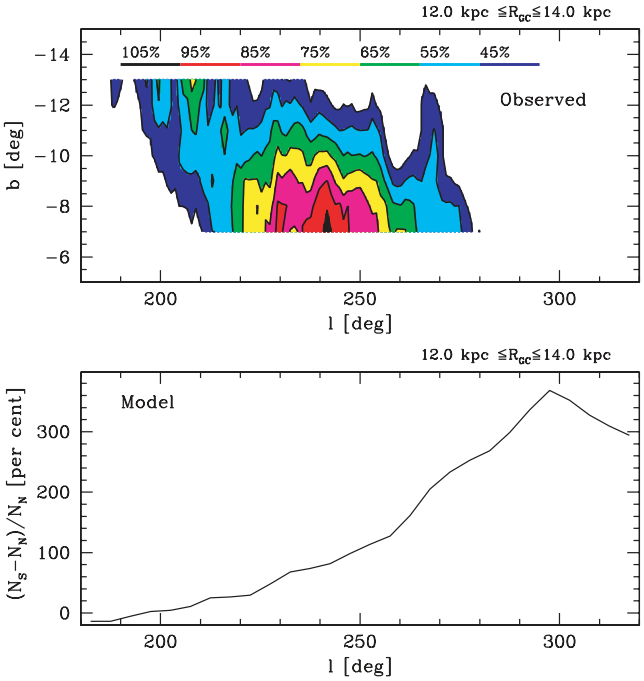

Figure 9. Upper panel: subtracted map (SN) in terms of fractional excess of surface density in the sky for RC stars in the range of Galactocentric distances $12.0 \leqslant R_{GC} \leqslant 14.0$ kpc, i.e. the range enclosing the densest part of the CMa structure. Lower panel: fractional density excess as a function of Galactic longitude in the same range of Galactocentric distances, as predicted by the López-Corredoira et al. warp model. Data for $|b| < 5^{\circ}.0$ are not included here.

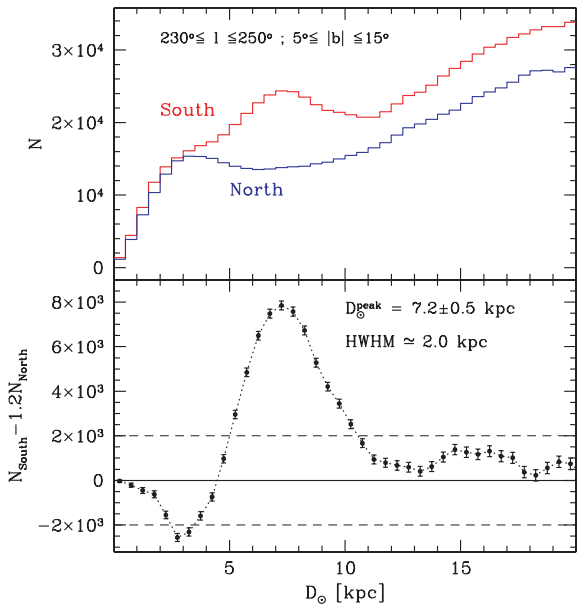

Figure 10. Distance profile of the Canis Major overdensity. Upper panel: distance distribution of RC stars in the range $230^{\circ} \leqslant l \leqslant 250^{\circ}$ and $5^{\circ} \leqslant |b| \leqslant 15^{\circ}$ in the Southern (red) and Northern (blue) Galactic hemisphere. Lower panel: residual of the subtraction of the rescaled Northern profile (by a factor of $\times 1.2$) from the Southern profile. The long-dashed lines approximately enclose the range of variation of the flat part of the residual in response to variations of the scaling factor by ± 10 per cent.

Section 4.3) is completely lost in the case of Argo. This strongly suggests that Argo is not a coherent stellar system, but is instead just a surface density structure that originates from the mix of different (and unrelated) populations that happen to lie along the same LOS.

RP05 discard the warp hypothesis for the nature of Argo claiming that the shape of the structure is not 'warp-like'. However, in their view, *all* the southern overdensities in the $220^{\circ} \leqslant l \leqslant 320^{\circ}$ region are due to Argo and CMa. The implicit conclusion is that the Galactic warp (and flare) does not produce any observable SN asymmetry in this region, at odds with the conclusions of L02 and Vig et al. (2005). The smooth nature of the global SN asymmetry shown to be present in this region, its Galactic-scale dimensions and the fact that a rescaled version of Northern density map is a good model for it (Fig. 5) strongly indicate that the surface density structure centred around $l = 290^{\circ}$ is not a dwarf galaxy remnant (Argo) but the effect of the warp (and flare) asymmetries of the Galactic disc.

Turning back our attention to CMa, there is an interesting point that can be appreciated from the comparison of Figs 9 and 10. While the CMa structure is present in both maps, its appearance is quite different. Most of the difference is just apparent and is due to the density scale adopted in Fig. 8, that is best suited to provide a good view of 'Argo' and compress the whole structure of CMa to just three levels of density. However, part of the difference is real, and is due to the much larger degree of foreground/background contamination affecting the map of Fig. 8, which includes stars at any Galactocentric distance. In particular, the centre of the structure (i.e. the region of maximum density) is shifted from $l \sim 242^{\circ}$ in the distance limited map (Fig. 9, that should be closer to the actual physical structure of the system) to $l \sim 244^{\circ}$ in the all-distances map of Fig. 8 due to contamination by likely unrelated stars at various distances along the LOS. This kind of effect should be always taken into account in studying the structure of CMa, since effects due to the *integration along the LOS* can significantly change the overall view of the system.

3.3 The nature of the Canis Major overdensity

In our view, there are only two possible explanations for the observational evidence presented above.

(i) Canis Major is a strong and unexpected substructure of the outer Galactic disc. This would imply that the disc hosts very dense and compact substructures of *old stars* [the age should be more than 1–2 Gyr to have RC stars and should be more than 4–5 Gyr according the optical CMDs; see Paper II and Martinez-Delgado et al. 2005a]. Such substructure should be very different, in nature, from usual spiral arms, for instance, that host populations dominated by very young stars. A local distortion of the outer disc, coupled with a large-scale warp, may also possibly reproduce the observed distribution of overdensities in the Southern Galactic hemisphere.

(ii) Canis Major is the remnant of a disrupting dwarf galaxy, as suggested in Papers I–IV. This interpretation naturally fits all the observational evidence collected up to now, with particular emphasis on the size and density of the structure and to the kinematics of its stars [see Paper III, Paper IV, Martinez-Delgado et al. (2005b) and Dinescu et al. (2005)].

For the reasons described above and in the previous papers of this series, our preference goes to the second hypothesis that appears to provide a much easier explanation of the whole observational scenario. In the following, we will take this hypothesis as true and,

on this basis, we will derive some interesting physical characteristics of CMa as a stellar system.

4 PHYSICAL PARAMETERS OF CANIS MAJOR

4.1 Distance

In Paper III, we obtained a distance profile of CMa using M giants as distance indicators. Here, we can repeat that analysis using the more reliable distance scale provided by RC stars. In the upper panel of Fig. 10, we show the distance distribution of the RC stars in our sample in the Northern (blue) and Southern (red) hemispheres, in a wide region towards the centre of CMa. The southern profile shows an overall excess at any distance, with respect to the northern one, plus an additional bump peaked around $D_\odot \simeq 7.5$ kpc. We rescaled the northern distribution by the same factor as in Fig. 5 (e.g. $\times 1.2$) and subtracted it from the southern profile. The result is shown in the lower panel of Fig. 10: the SN excess appears to be confined within $D_\odot \simeq 5$ kpc and $D_\odot \sim 12$ kpc. The peak of the profile is at $D_\odot = 7.2 \pm 1.0$ kpc and the HWHM is $\simeq$2.0 kpc, in excellent agreement with the results of Paper I, Paper III and Martinez-Delgado et al. (2005a). There are a few interesting considerations that can be deduced by inspecting Fig. 10.

(i) The distance profile of CMa as obtained from its RC stars is strikingly similar to that derived from M giants in Paper III. Even leaving aside the perfect coincidence of the peaks of the two distributions that may be ascribed to a mere coincidence within the uncertainties associated with the two distance scales, it remains a fact that the two independent tracers give essentially *the same* LOS profile of the CMa system.

(ii) In our various analyses, we have obtained distance estimates for CMa from four different and independent distance indicators. In order of accuracy: from the tip of the red giant branch in the *I* band ($D_\odot \simeq 7.2$ kpc; Paper III), from the RC in *K* band ($D_\odot \simeq 7.2$ kpc, present analysis), from the photometric parallax of M giants in the *K* band ($D_\odot \simeq 7.1$ kpc; Paper I), and from MS fitting in the *B* and *V* bands ($D_\odot \simeq 7.6$–8.7; Paper II). All of these independent methods consistently provide a distance of the centre of CMa within 7.0 and 9.0 kpc. Hence, the average distance of CMa should be now regarded as a very reliable piece of information about this system. Note that if $D_\odot \simeq 7.2$ kpc is assumed, the age estimate obtained in Paper II would shift towards older ages (i.e. 6 Gyr $\lesssim$ age $\lesssim$ 10 Gyr, instead of 4 Gyr $\lesssim$ age $\lesssim$ 10 Gyr).

4.1.1 The spatial orientation of CMa

The subtracted density maps of Figs 3, 5 and 6 make evident that the physical orientation of the elongated body of CMa implies a heliocentric distance–longitude gradient: the heliocentric distance of CMa grows with Galactic longitude. Using the same technique as above, we find that the distance of the main body of CMa varies from $D_\odot \simeq 6.3$ kpc at $l \simeq 225^\circ$, to $D_\odot \simeq 7.2$ kpc at $l \simeq 240^\circ$, to $D_\odot \simeq 9.3$ kpc at $l \simeq 265^\circ$.

The effect is clearly depicted in Fig. 11, where the contours of the main body of CMa [in red, taken from Fig. 5(b)] are superposed on the results of the *N*-body simulation of the disruption of the CMa galaxy presented in Paper IV. The simulation is produced by a dwarf galaxy model of mass $5 \times 10^8\,M_\odot$ that is accreted on to the Milky Way during $\sim$3 Gyr (see Paper IV for details) and it was built to reproduce the current mean position and 3D velocity of CMa as well as the *distance–radial velocity* gradient discovered in Paper IV.

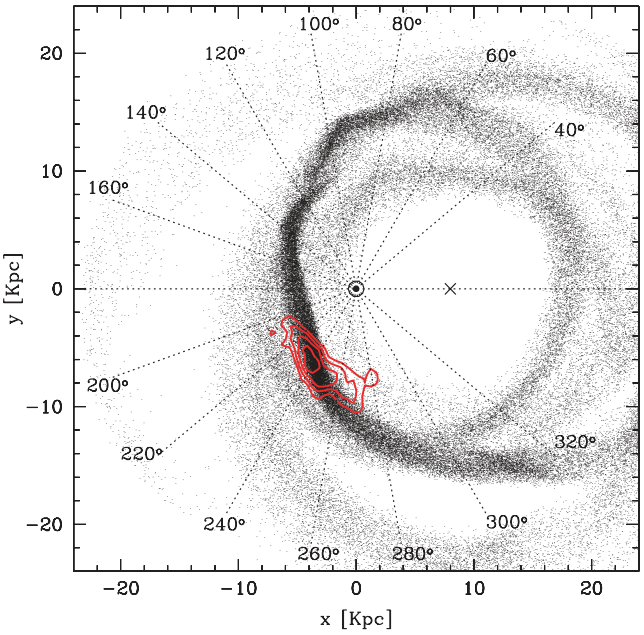

Figure 11. The excess-density contours of CMa taken from Fig. 5(b) (down to 16σ, in red) are compared with the *N*-body model of the disruption of the CMa presented in Paper IV (small dots).

Hence, the *distance–longitude* behaviour of the remnant is a *prediction* of the model, and not an a priori requirement. Therefore, the excellent qualitative and quantitative agreement with the *observed* and *predicted* spatial orientation of the main body of CMa may be considered as a success of the dwarf-galaxy-accretion scenario for the nature of CMa. In other words, the structure and spatial orientation of CMa as obtained from RC stars are fully consistent with the model of a disrupting dwarf galaxy that fits the observed position and kinematics of CMa.

4.2 Luminosity and surface brightness

The evolutionary flux relation (Renzini & Buzzoni 1986; Renzini & Fusi Pecci 1988; Renzini 1998) states that the total number of stars in a given evolutionary phase $j(N_j)$ is proportional to the total luminosity of a stellar system (L_T). Considering a simple stellar population (SSP, i.e. a population of stars with the same age and chemical composition):

$$N_j = B(t) L_T t_j, \tag{4}$$

where t_j is the duration of the evolutionary phase in years, and $B(t)$ is the specific evolutionary flux, i.e. the number of stars entering or leaving any post MS evolutionary phase per year per solar luminosity as a function of time (t, i.e. the age of the SSP).

We can use equation (4) to obtain a distance-independent estimate of the total luminosity of CMa from the RC star counts. With some algebra, we obtain

$$M_V = -2.5 \left\{ \log[N_j] - \log\left[\frac{L_T}{L_V}\right] - \log[t_j] - \log[B(t)] \right\} + M_{V\odot}, \tag{5}$$

where M_V is the absolute integrated magnitude in the V band and $M_{V\odot}$ is the absolute V magnitude of the Sun. For the present case, we adopt $B(t) = 1.71 \times 10^{-11}$ and $\frac{L_T}{L_V} = 1.5$ from the SSP models by Maraston (1998, 2005) with $[M/H] = -0.33$, age $= 6.0$ Gyr

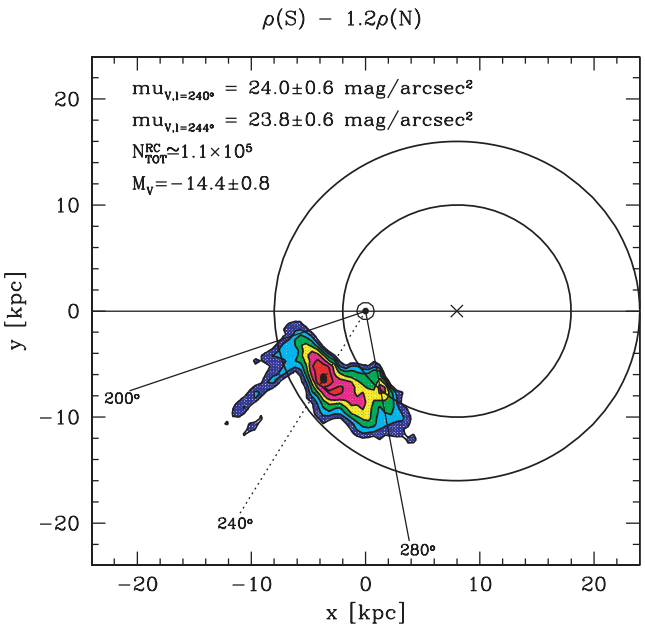

Figure 12. Subtracted density map taken from Fig. 5(a) (Northern hemisphere densities rescaled by a factor of ×1.2). The continuous circles with radius $R_{GC} = 10.0$ and 16.0 kpc, and the continuous lines indicating the directions $l = 200^\circ$ and $l = 280^\circ$ enclose the region that we have considered for the computation of the total number and the central surface density of RC stars attributable to Canis Major. These numbers have been used to compute the integrated absolute magnitude and the surface brightness (towards two different directions) of the system that are reported in the figure.

and Salpeter Initial Mass Function.[1] $M_{V\odot} = 4.83$ is also adopted according to Maraston (1998), while the duration of the core He-burning phase ($t_{HB} = 0.87 \times 10^8$ yr) for a population with age ≃6.0 Gyr and $[M/H] = -0.35$ has been taken from Pietrinferni et al. (2004).[2]

In the same way, we can use equation (5) by Renzini (1998) to obtain a distance-dependent estimate of the surface brightness near the centre of CMa ($\mu_{V,0}$):

$$\mu_{V,0} = -2.5\log(n_j) + 2.5\log(\mathrm{FoV}) + (m - M)_0 + \mathrm{Norm}, \qquad (6)$$

where n_j is the number of stars in the j evolutionary phase within the considered field of view (FoV, in arcsec ^{2}, for example), and the term *Norm* encompasses all the theoretical assumptions:

$$\mathrm{Norm} = 2.5\log\left[\frac{L_T}{L_V}\right] + 2.5\log[t_j] + 2.5\log[B(t)] + M_{V\odot}.$$

We assume the distance modulus $(m - M)_0 = 14.3$ as derived in Paper III and in the present contribution.

To estimate the observables required by equations (5) and (6) (N_{HB} and n_{HB}), we proceeded as follows. We selected from our sample the RC stars of both hemispheres within $200^\circ \leqslant l \leqslant 280^\circ$, $15\overset{\circ}{.}0 \leqslant |b| \leqslant 5\overset{\circ}{.}0$ and $10.0 \leqslant R_{GC} \leqslant 16.0$ kpc (the adopted selection is displayed in Fig. 12). Then, we subtracted the total number of Northern RC stars – rescaled by the usual 1.2 factor – from the total number of Southern RC stars in this region. We obtain an excess of $\simeq 1.1 \times 10^5$ RC stars that can be associated to CMa, corresponding to a total luminosity of $L_T \simeq 7.4 \times 10^7\, L_\odot$. The integrated absolute magnitude is $M_V = -14.4 \pm 0.8$, where the uncertainty includes a ±10 per cent variation in the ×1.2 scaling factor adopted to take into account the contribution of the large-scale overdensity (warp) to the detected excess. This estimate is in excellent agreement with those obtained in Paper I from M giants and by Martinez-Delgado et al. (2005a) from optical photometry ($M_V = -14.5 \pm 0.1$). We estimate that the inclusion or exclusion from the sample of the stars within the $|b| < 5^\circ$ region may change the value of the V-band integrated magnitude by $\sim \pm 0.5$ mag.

To estimate the surface brightness, we computed the ρ(S)–1.2 ρ(N) excess of RC stars within a $2^\circ \times 2^\circ$ box centred on $(l, b) = (240^\circ, -6^\circ)$ and on $(l, b) = (244^\circ, -6^\circ)$. We chose two different positions to provide estimates of the surface brightness for the centre of the structure as obtained from a distance-selected sample (as in Fig. 9) and from the straight surface density distribution, as in Fig. 8. We obtain a density of ≃314 RC stars deg^{-2} at $l = 240^\circ$, corresponding to $\mu_V = 24.0 \pm 0.6$ mag arcsec^{-2}, and ≃370 RC stars deg^{-2} at $l = 244^\circ$, corresponding to $\mu_V = 23.8 \pm 0.6$ mag arcsec^{-2}. These values are in reasonable agreement with the results of Martinez-Delgado et al. (2005a) obtained from data at $(l, b) = (240^\circ, -8^\circ)$ ($\mu_{V,0} = 23.3 \pm 0.1$ mag arcsec^{-2}).

Note that $B(t)$, at fixed $[M/H] = -0.33$, varies from 1.66×10^{-11} at $t = 1.0$ Gyr to 1.75×10^{-11} at $t = 13.0$ Gyr, and, for fixed age = 6.0 Gyr, it ranges from 1.66×10^{-11} at $[M/H] = -1.35$ to 1.98×10^{-11} at $[M/H] = +0.35$. The variation of t_{HB} over the same range of age and metallicity is just of a few per cent (Pietrinferni et al. 2004). Hence, the particular choices of the above parameters do not seriously affect our final estimates. Other factors, not completely accounted for, as the uncertainty in the exact position of the centre of CMa, the overall extent of the system and the adopted SSP hypothesis are expected to be the dominant contributors to the uncertainty of our estimates of the integrated magnitude and of the central surface brightness of the system.

CMa turns out to have a total luminosity and a surface brightness quite similar to those of the Sgr dSph, as already noted in Paper I, but the above results suggest that it may be slightly more luminous and with a brighter $\mu_V, 0$, in agreement with the M_V versus $\mu_V, 0$ relation of dwarf spheroidal galaxies (see Martinez-Delgado et al. 2005a, and references therein).

It is interesting to note the striking effect of the relative distance on the number densities for two stellar systems of similar central surface brightness. Monaco et al. (2003) measured a density of RC stars of ≃2100 deg^{-2} in the central degree of the Sgr dSph, while here we observe just 314 deg^{-2} at $l = 240^\circ$, yet the surface brightness of the two systems is similar. This may largely account for the great difficulty in the identification of the RC of CMa in optical CMDs from off-centred fields of 0.25 deg^2 or less as those presented in Paper II and in Martinez-Delgado et al. (2005a). This argument will be developed further in Section 4.4.

4.3 How should a nearby galaxy appear?

CMa is by far the nearest dwarf galaxy known, a factor of ≃3.6 closer than the previous 'record holder', the Sgr dSph (Monaco et al. 2004). This is the main reason why it appears so unusual at the first glance: a structure covering tens of degrees on the sky and with as few as ∼300–400 RC stars in its central square degree. This is very far from our idea of the typical dwarf satellite of the Milky Way that has been acquired by studying much more distant examples. To show that there is nothing unusual in CMa except its distance, we undertook the exercise of seeing how the Sgr dSph galaxy would appear if it were placed at the same distance and position as CMa.

[1] see http://www.mpe.mpg.de/maraston/SSP
[2] see http://www.te.astro.it/BASTI/

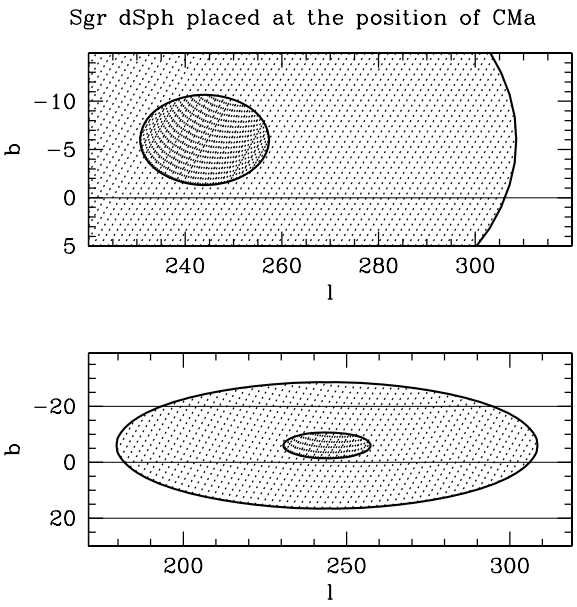

Figure 13. The appearance of the Sgr dSph if it were placed at the distance and position of CMa. The inner ellipse encloses the core of the galaxy (densely shaded region), and the outer ellipse is the limiting contour [sparsely shaded region; Sgr parameters from Majewski et al. (2003)]. The upper panel has the same longitude scale as in Fig. 8 to allow a direct comparison with the map shown there.

In the following, we will adopt the structural parameters of Sgr (core radius r_c, limiting radius r_t, central surface brightness and axis ratio) as derived by Majewski et al. (2003), the distance from Monaco et al. (2004) and the surface density of Horizontal Branch stars from Monaco et al. (2003).

Fig. 13 shows the core and the limiting contours of Sgr once placed at the distance and position of CMa. The upper panel of Fig. 13 has the same longitude scale as Fig. 9, to allow a direct comparison. The core of the 'mock' Sgr shows a major axis of more than $\sim 26^\circ$ ($r_c = 13\overset{\circ}{.}3$), and the overall appearance is strikingly similar to CMa. Note that the limiting contour extends well beyond $l = 200^\circ$ on the low-longitude side, and beyond $l = 300^\circ$ on the other ($r_t = 64\overset{\circ}{.}5$). Note also that the outskirts of the 'mock' Sgr galaxy extends into the Northern Galactic hemisphere, up to $b \sim +5/10^\circ$.

From equation (6), the following relation can be derived between the surface brightness (at any chosen wavelength λ) $\mu_{\lambda,1}$, $\mu_{\lambda,2}$ and the number of stars per given area in a given evolutionary phase (n_1, n_2) for two stellar systems located at distances d_1 and d_2:

$$\mu_{\lambda,1} - \mu_{\lambda,2} = -2.5 \log(n_1/n_2) + 5 \log(d_1/d_2). \quad (7)$$

The second term on the right-hand side of equation (7) displays the effect of distance on the number surface density of a system of a given surface brightness.[3] To rescale the number surface density of Sgr from $d_2 = 26.3$ kpc to $d_1 = 7.2$ kpc, we must assume $\mu_{\lambda,1} - \mu_{\lambda,2} = 0.0$. In the present case, we find that the observed surface number density of Sgr stars should be reduced by a factor of 0.075, if the galaxy is placed at the distance of CMa. Hence, in this case, we would observe $\sim$150 RC stars deg^{-2}, 10 RR Lyrae deg^{-2} and 12 Blue Horizontal Branch stars deg^{-2} in the centre of the Sgr galaxy. This effect fully accounts for the difficulty of detecting clearly defined sequences of evolved stars in small fields (smaller than 1 deg^2) even within the main body of CMa, as well as for the low yield in searches of rare stellar species (as RR Lyrae stars in a system dominated by an intermediate-age and metal-rich population; see Kinman et al. 2004; Mateu et al. 2005).

In conclusion, the apparent size of CMa and the number density of its stellar populations are fully compatible with those of a dwarf galaxy similar to Sgr and located at 7.2 kpc from us.

[3] It has to be noted that the effect of the physical size of a system on the spread of sequences on a CMD weakens with increasing distance. This is an additional factor that favours the easier recognition of distant stellar structures compared to more nearby systems.

4.4 Old open clusters in CMa

The possible association of some old open clusters with CMa was already suggested in Paper I (see also Paper II; Crane et al. 2003; Frinchaboy et al. 2004). A thorough analysis of these clusters is clearly beyond the scope of the present contribution. However, the use of the RC as a tracer may provide a unique opportunity of placing a few clusters on to the same distance scale as the field population of CMa. In Table 1, we list a number of open clusters selected to be older than $\sim$0.8 Gyr and to lie in the surroundings of the main body of CMa [according to the WEBDA data base (http://www.univie.ac.at/webda); Mermilliod 1995]. In particular, the first group presented in Table 1 is composed of three clusters that directly project on to the main body of CMa (as seen in Figs 8 and 10, for instance), and for which it has been possible to estimate the K magnitude of the RC from 2MASS photometry. Hence, the distance estimates for To 2, AM 2 and Haf 11 have been derived in exactly the same way and under the same assumptions (luminosity of the standard candle and reddening) used for the analysis of the field population performed above. These estimates strongly indicate that To 2, AM 2 and Haf 11 are physically located within the main body of CMa (see Paper II for further discussion and references). Note that while AM 2 and Haf 11 lack any radial velocity estimate, To 2 has $V_r \simeq +114$ km s^{-1}, fully consistent with the systemic velocity of CMa (Paper III; Paper IV).

5 SUMMARY AND CONCLUSIONS

We have performed a differential analysis of the distribution of the Southern Galactic hemisphere excess of colour-selected RC stars extracted from 2MASS in the region $40^\circ \leqslant l \leqslant 320^\circ$ and $5^\circ \leqslant |b| \leqslant 15^\circ$. Our main aim was to trace the structure of the main body of the newly discovered Canis Major stellar system (Paper I) and of the stellar component of the southern part of the Galactic warp (Paper II; Paper III).

We have obtained detailed maps of the SN and NS overdensities in the Galactic disc. These maps show that the third and fourth Galactic quadrants ($180^\circ \leqslant l \leqslant 360^\circ$) are dominated by a smooth large-scale SN asymmetry that extends all over the considered half of the disc and over a large range of heliocentric distances. The above characteristics, the comparisons with the large-scale NS asymmetries observed in the first and second quadrants ($0^\circ \leqslant l \leqslant 180^\circ$) and the comparison with the warped and flared Galactic model of L02 strongly suggest that such a wide SN overdensity is due to an asymmetry of Galactic scale, in particular the southern lobe of the warp of the Galactic disc.

The Canis Major structure, as recognized in Paper I and Paper II, appears – in the SN density maps – as the strongest *spatial* overdensity of the whole Galactic disc in terms of either number density or statistical significance. Simply subtracting a rescaled version of

Table 1. Old open clusters around the main body of CMa.

Name	l°	b°	$E(B-V)$	$K_0^{\rm RC}$	$(m-M)_0$	$D_\odot$ (kpc)
Tombaugh 2	232.83	−6.88	0.29	12.95 ± 0.10	14.45 ± 0.22	7.76 ± 0.8
Haffner 11	242.39	−3.54	0.57	12.20 ± 0.20	13.70 ± 0.28	5.49 ± 0.8
Arp-Madore 2	248.12	−5.88	0.51	13.65 ± 0.10	15.15 ± 0.22	10.71 ± 1.1
Berekeley 36	227.38	−0.59				6.1
NGC 2243	239.48	−18.01				4.4
Melotte 66	259.56	−14.24				4.3
Ruprecht 75	276.79	−4.48				4.3
CC06	238.48	−4.28				4.5
Van den Bergh-Hagen 66	276.00	−3.01				7.0
Saurer 2	257.99	−1.01				4.8

All the reported data, with the exception of those relative to the RC distance of To 2, AM 2 and Haf 11, are drawn from the WEBDA data base (Mermilliod 1995); see http://obswww.unige.ch/webda/. Data for CC06 are from Ivanov et al. (2002). First group: clusters within $230^\circ \leqslant l \leqslant 260^\circ$, $-12^\circ \leqslant b \leqslant 3^\circ$ and 4.0 kpc $\leqslant D_\odot \leqslant$ 11.0 kpc, with age $\geqslant$1 Gyr. Second group: clusters within $220^\circ \leqslant l \leqslant 280^\circ$, $-20^\circ \leqslant b \leqslant 0^\circ$ and 4.0 kpc $\leqslant D_\odot \leqslant$ 11.0 kpc, with age $\gtrsim$0.8 Gyr.

the Northern hemisphere density map (by a factor of 1.2) from the Southern hemisphere density map, the large-scale asymmetry attributable to the Galactic warp is completely removed, and Canis Major remains as the only significant overdensity, with a peak at more than 25σ. The structure appears elongated along the tangential direction, extending from $l \simeq 200^\circ$ to $\simeq 280^\circ$. It has a nearly elliptical shape and it is strongly spatially confined, with a HWHM along the LOS at its centre of $\simeq$2.0 kpc (in excellent agreement with the results of Paper I, Paper III and Martinez-Delgado et al. 2005a). All the maps show that Canis Major has a roundish core, located at $D_\odot = 7.2 \pm 1.0$ kpc, towards $l = 241\overset{\circ}{.}7$, at a Galactocentric distance of $R_{\rm GC} = 13.1 \pm 1.0$ kpc.

The L02 model of the Galactic warp is unable to predict the existence of Canis Major as a structure of Galactic origin, both on the large and on the local scale. The same has been shown to be true also for the Yusifov (2004) and the R03 models, in Paper III and in Paper II, respectively (also see Fig. 1). Within the framework set by the observational evidence listed above, Canis Major appears as a compact and confined stellar system that is 'superposed' on the warp structure (see Fig. 3, for example).

We also investigate the claim made in the recent study by RP05, that Canis Major is an external field of a larger Argo structure, which would be the true centre of the dwarf galaxy remnant accreted on to the Milky Way. The distribution of RC stars along the LOS does not support this conclusion, however. Unlike the situation in the Canis Major region, we find no significant spatially confined structure in the LOS through Argo. This LOS, instead, crosses the region of the disc where the large-scale overdensity associated with the Galactic warp reaches its maximum. We conclude that Argo is most likely not related to Canis Major, and is probably an asymmetry of Galactic origin.

The above observational scenario does not provide the ultimate word on the nature of CMa. Given our poor knowledge of the outermost region of the Galactic disc and the obvious limitations in current models of the disc itself, the possibility that CMa is a substructure of the Galactic disc cannot be excluded yet. However, in this case, we should admit the presence of an unexpected large and very dense substructure and/or local distortion in the outer disc, hosting essentially *old* stars, at odds with, for instance, usual spiral arms.

In our view, the evidence collected here, in Paper I, in Paper II and by Martinez-Delgado et al. (2005a), together with the kinematics of Canis Major stars as described in Paper III, Paper IV and the possible links with the Monoceros Ring (Paper I; Paper IV, Conn et al. 2005b; Dinescu et al. 2005; Martinez-Delgado et al. 2005b; Penarrubia et al. 2005) are more naturally explained by the hypothesis that Canis Major is the remnant of the disrupting dwarf galaxy in a nearly circular and nearly planar orbit about the centre of the Galaxy. Accepting this hypothesis as the one that best fits all the available data, we have derived several physical characteristics of CMa as a stellar system that are summarized in Table 2. In particular, we draw the attention of the reader on the following specific results of the present analysis.

Table 2. Fundamental parameters of the main body of the Canis Major system.

$\langle D_\odot \rangle$	7.2 ± 1.0 kpc
$l_0{}^a$	$244\overset{\circ}{.}0 \pm 2\overset{\circ}{.}0$
$b_0{}^b$	$-6\overset{\circ}{.}0 \pm 1\overset{\circ}{.}0$
$\langle R_{\rm GC} \rangle$	13.1 ± 1.0 kpc
x	3.7 ± 0.6 kpc
y	-6.4 ± 0.6 kpc
z	$\simeq -0.8$ kpc
M_V	-14.4 ± 0.9 mag
$\mu_{V,240^\circ}$	24.0 ± 0.6 mag arcsec^{-2}
$\mu_{V,244^\circ}$	23.8 ± 0.6 mag arcsec^{-2}
HWHM$_{\rm LOS}$	$\simeq$2.0 kpc

[a] As derived from Fig. 8. Adopting the distance selected sample of Fig. 10, $l_0 = 241\overset{\circ}{.}7 \pm 1\overset{\circ}{.}0$ is obtained (see Section 3.2.1).
[b] As derived from Fig. 8.

(i) RC stars provide a quantitative description of CMa that is in full agreement with those obtained from other independent tracers (M giants and MS stars, see Paper I, Paper II, Paper III and Martinez-Delgado et al. 2005a). In particular, we obtained an (distance-independent) estimate of the integrated V magnitude and an (distance-dependent) estimate of the central surface brightness in good agreement with those obtained by Martinez-Delgado et al. (2005a) from deep optical photometry of MS stars. We also obtained a distance profile (along the LOS) of CMa that is essentially indistinguishable from that obtained in Paper III from M giants. The high degree of self-consistency achieved among the various analyses – using different tracers – may be considered also as a validation of our criterion of selection of RC stars. We confirm, with independent

tracers and an independent distance scale with respect to Paper I and Paper III, that the mean distance of CMa is $D_{\odot} = 7.2 \pm 1.0$ kpc, around $l = 240^{\circ}$.

(ii) We have detected a clear relation between the mean distance to CMa and Galactic longitude within the main body. The derived spatial orientation of the system is in good agreement with the predictions of the *N*-body simulation presented in Paper IV, that models CMa as a dwarf galaxy being accreted in a planar orbit on to the disc of the Milky Way.

(iii) Using the same data set (2MASS), the same tracer (RC stars) and the same distance scale as in the analysis summarized above, we showed that the old open clusters AM 2, To 2 and Haf 11 are located (in space) within the main body of Canis Major.

In summary, the present study fully (and independently) confirms the results presented in previous papers of this series and in Martinez-Delgado et al. (2005a): Canis Major has the size, the luminosity and the kinematics typical of a large dwarf galaxy, seen during the last stages of its disruption within the tidal field of the Milky Way (see also Sbordone et al. 2005). While a Galactic origin for CMa cannot be definitely ruled out with the present data, the dwarf galaxy hypothesis appears as best suited to fit the overall observational scenario.

While further details emerge – as, for example, the distance–longitude gradient – we begin to obtain a clearer view of this challenging system. Future studies should try to overcome the several observational challenges posed by this nearby, low-latitude object, to unveil the details of its stellar content (age, chemical composition) and to clarify its possible connection with the Monoceros Ring.

ACKNOWLEDGMENTS

The financial support of ASI and MIUR is acknowledged. MB is grateful to the ULP/Observatoire de Strasbourg for the kind hospitality during a period in which a significant part of the analysis presented in this paper was performed. The referee, M. López-Corredoira, is acknowledged for his very helpful comments that led us to a much deeper analysis of the scientific problems considered here. This publication makes use of data products from the 2MASS, which is a joint project of the University of Massachusetts and the Infrared Processing and Analysis Centre/California Institute of Technology, funded by the National Aeronautics and Space Administration and the National Science Foundation. This research has made use of NASA's Astrophysics Data System Abstract Service. This research has made use of the WEBDA database, operated at the Institute for Astronomy of the University of Vienna. The assistance of P. Montegriffo in the development of the software required for the present analysis is also acknowledged.

REFERENCES

Abadi M. G., Navarro J. F., Steinmetz M., Eke V. R., 2003a, ApJ, 591, 499
Abadi M. G., Navarro J. F., Steinmetz M., Eke V. R., 2003b, ApJ, 597, 21
Babusiaux C., Gilmore G., 2005, MNRAS, 358, 1309
Bellazzini M., Ferraro F. R., Ibata R., 2003a, AJ, 125, 188
Bellazzini M., Ibata R., Ferraro F. R., Testa V., 2003b, A&A, 405, 577
Bellazzini M., Ibata R., Monaco L., Martin N., Irwin M. J., Lewis G. F., 2004a, MNRAS, 354, 1263 (Paper II)
Bellazzini M., Ferraro F. R., Sollima A., Pancino E., Origlia L., 2004b, A&A, 424, 199
Binney J., 1992, ARAA, 30, 51
Bonifacio P., Monai S., Beers T. C., 2000, AJ, 120, 2065
Brown J. A., Wallerstein G., Geisler D., Oke J. B., 1996, AJ, 112, 1551
Carraro G., Vàzquez R. A., Moitinho A., Baume G., 2005, ApJ, 630, L153
Cole A. A., 2001, ApJ, 559, L17
Conn B., Lewis G. F., Irwin M. J., Ibata R. A., Irwin J. M., Ferguson A. M. N., Tanvir N., 2005a, MNRAS, 362, 475
Conn B., Martin N., Lewis G. F., Ibata R. A., Bellazzini M., Irwin M. J., 2005b, MNRAS, 362, 475
Crane J. D., Majewski S. R., Rocha-Pinto H., Frinchaboy P. M., Skrutskie M. F., Law R. D., 2003, ApJ, 594, L119
Cutri et al., 2003, Explanatory Supplement to the 2MASS All Sky Data Release. Online publication only: http://www.ipac.caltech.edu/2mass/releases/allsky/doc/explsup.html
Dinescu D. I., Martínez-Delgado D., Girard T. M., Penarrubia J., Rix H. W., Butler D., van Altena W. F., 2005, ApJ, 631, L49
Djorgovski S., Sosin C., 1989, ApJ, 341, L13
Ferraro F. R., Messineo M., Fusi Pecci F., de Palo A., Straniero O., Chieffi A., Limongi M., 1999, AJ, 118, 1738
Forbes D. A., Strader J., Brodie J. P., 2004, AJ, 127, 3394
Frinchaboy P. M., Majewski S. R., Crane J. D., Reid I. N., Rocha-Pinto H. J., Phelps R. L., Patterson R. J., Muñoz R. R., 2004, ApJ, 602, L21
Hammersley P. L., Garzon F., Mahoney T., Calbet X., 1995, MNRAS, 273, 206
Helmi A., 2004, ApJ, 610, L97
Helmi A., White S. D. M., Springel V., 2003, MNRAS, 339, 834
Helmi A., Navarro J., Meza A., Steinmetz M., Eke V., 2003, ApJ, 592, L25
Ibata R., Lewis G., 1998, ApJ, 500, 575
Ibata R. A., Wyse R. F. G., Gilmore G., Irwin M. J., Suntzeff N. B., 1997, AJ, 113, 634
Ibata R., Lewis G., Irwin M., Totten E., Quinn T., 2001, ApJ, 551, 294
Ibata R., Lewis G., Irwin M., Cambrésy L., 2002, MNRAS, 332, 921
Ibata R., Irwin M., Lewis G., Ferguson A., Tanvir N., 2003, MNRAS, 340, L21
Ivanov V. D., Borissova J., Pessev P., Ivanov G. R., Kurtev R., 2002, A&A, 394, 1
Ivezic Z. et al., 2000, AJ, 120, 963
Johnston K. V., Law D. R., Majewski S. R., 2005, ApJ, 619, 800
Kinman T. D., Saha A., Pier J. R., 2004, ApJ, 605, L25
Kubiak M., Kaluzny J., Krzemińsky W., Mateo M., 1992, Acta Astron., 42, 155
Kuijken K., Garcia-Ruiz I., 2001, in Funes J. G., S. J., Corsini E. M., eds, ASP Conf. Ser. Vol. 230, Galaxy Disks and Disk Galaxies. Astron. Soc. Pac., San Francisco, p. 401
López-Corredoira M., Cabrera-Lavers A., Garzón F., Hammersley P. L., 2002, A&A, 394, 883
Law D. R., Johnston K. V., Majewski S. R., 2005, ApJ, 619, 807
Majewski S., Skrutskie M., Weinberg M., Ostheimer J., 2003, ApJ, 599, 1082
Maraston C., 1998, MNRAS, 300, 872
Maraston C., 2005, MNRAS, 362, 799
Martin N., Ibata R. A., Bellazzini M., Irwin M. J., Lewis G. F., Dehnen W., 2004a, MNRAS, 348, 12 (Paper I)
Martin N., Ibata R. A., Bellazzini M., Conn B., Irwin M. J., Lewis G. F., McConnachie A. W., 2004b, MNRAS, 355, L33 (Paper III)
Martin N., Ibata R. A., Conn B., Lewis G. F., Bellazzini M., Irwin M. J., 2005, MNRAS, 362, 906 (Paper IV)
Martinez-Delgado D., Butler D. J., Rix H.-W., Franco I., Penarrubia J., 2005a, ApJ, 633, 205
Martinez-Delgado D., Penarrubia J., Dinescu D., Butler D. J., Rix H.-W., 2005b, in Jerjen H., Binggeli B., eds, IAU Coll. 198, Near field Cosmology with Dwarf Elliptical Galaxies. in press (astro-ph/0506012)
Mateo M., 1998, ARA&A, 36, 435
Mateu C. E., Vivas A. K., Zinn R., Miller L., 2005, in Abad C., Bongiovanni A., Guillen Y., eds, Internat. Workshop Astronomia Dinamica en Latino-America (ADeLA 2004). Rev. Mex. A. A. Conf Ser., in press (astro-ph/0504333)
Mermilliod J.-C., 1995, in Egret D., Albrecht M. A., eds, Information and On-Line Data in Astronomy. Kluwer, Dordrecht, p. 127
Monaco L., Bellazzini M., Ferraro F. R., Pancino E., 2003, ApJ, 597, L25

Monaco L., Bellazzini M., Ferraro F. R., Pancino E., 2004, 353, 874
Momany Y., Zaggia S. R., Bonifacio P., Piotto G., De Angeli F., Bedin L. R., Carraro G., 2004, A&A, 421, L29 [M04]
Morrison H. L., Mateo M., Olszewski E. W., Harding P., Dohm-Palmer R. C., Freeman K. C., Norris J. E., Morita M., 2000, AJ, 119, 2254
Newberg H. et al., 2002, ApJ, 569, 245
Newberg H. et al., 2003, ApJ, 596, L191
Paczynski B., Stanek K., 1998, ApJ, L219
Penarrubia J., Martinez-Delgado D., Rix H.-W. et al., 2005, ApJ, 626, 128
Pietrinferni A., Cassisi S., Salaris M., Castelli F., 2004, ApJ, 612, 168
Porcel C., Battaner E., Jiménez-Vicente J., 1997, A&A, 322, 107
Renzini A., 1998, AJ, 115, 2459
Renzini A., Buzzoni A., 1986, in Chiosi C., Renzini A., eds, Spectral evolution of galaxies. Reidel, Dordrecht, p. 135
Renzini A., Fusi Pecci F., 1988, ARAA, 26, 1999
Rieke G. H., Lebofsky M. J., 1985, ApJ, 290, 116
Robertson B., Bullock J. S., Font A. S., Johnston K. V., Hernquist L., 2005, ApJ, 632, 872
Robin A. C., Reylé S., Derrière S., Picaud S., 2003, A&A, 409, 523 (R03)
Rocha-Pinto H., Majewski S., Skrutskie M., Crane J., 2003, ApJ, 594, L115
Rocha-Pinto H., Majewski S., Skrutskie M., Patterson R. J., 2005, ApJ, submitted (astro-ph/0504122) (RP05)
Salaris M., Girardi L., 2002, MNRAS, 337, 332
Sarajedini A., Grochlski A. J., Levine J., Lada E., 2002, AJ, 124, 2625
Sbordone L., Bonifacio P., Marconi G., Zaggia S., Buonanno R., 2005, A&A, 430, L13
Schlegel D., Finkbeiner D., Davis M., 1998, ApJ, 500, 525 (SFD98)
Vig S., Ghosh S. K., Ojha D. K., 2005, A&A, 436, 867
White S., Rees M., 1978, MNRAS, 183, 341
White S., Frenk C., 1991, ApJ, 379, 52
Yanny B. et al., 2003, ApJ, 588, 824
Yusifov I., 2004, in Uyaniker B., Reich W., Wielebinski R., eds, The Magnetized Interstellar Medium. Copernicus GmbH, Katlenburg–Lindau, p. 165

APPENDIX A: CONTAMINATION BY DWARFS

To study the effect of the contamination by dwarfs in our colour-selected sample of candidate RC stars on subtracted density maps, we recur to the Galactic model by R03. This model includes the effect of the Galactic warp and of the disc flaring, and takes into account the off-plane position of the Sun. The main advantages of using the R03 model for our purpose can be summarized as follows.

(i) We can obtain (K, $J-K$) CMDs of the synthetic samples, therefore we can apply exactly the same selections and analysis adopted for the observed sample.

(ii) Synthetic stars from the R03 models are individually classified into different species with the flag *cl*, hence the discrimination of dwarfs from giants is straightforward. In particular, stars having $cl = 3$ are giants, those with $cl = 4$ are subgiants and those with $cl = 5$ are dwarfs. Since the synthetic CMDs reveal that both $cl = 4$ and 5 stars can fall into our selection colour window, from now on we will consider all the stars of class 4 or 5 as *dwarfs*.

The obvious disadvantage is that the result will not reflect the *real* Galaxy but just a model of it. However, in the present context, the unavoidable approximations inherent to a Galactic model should not represent a major concern. In the following, we will mainly focus on the magnitude range $12.0 \leqslant K \leqslant 14.0$, that is the range enclosing essentially all the stars that contribute to the main structures we discuss in the present paper, and CMa in particular.

To allow the possibility of a direct comparison with observed CMDs (a very useful sanity check) and to limit the dimensions of the synthetic catalogues, we choose to work on 30 deg^2 windows in the latitude range $6^\circ \leqslant |b| \leqslant 11^\circ$, i.e. exactly the same as the observed sample whose CMD is shown in Fig. 1. To study the dwarf contamination towards different directions of interest, we selected three windows at $l = 180^\circ \pm 3^\circ$, $241^\circ \pm 3^\circ$ (i.e. the same as Fig. 1) and $280^\circ \pm 3^\circ$. We extracted from the model the corresponding samples in the Southern and Northern Galactic hemispheres, at the above longitudes, for a total of six catalogues. The extraction was performed using the *large field* option that takes into account the variations of the population across the considered fields.[4] To reproduce as much as possible the real case, we let the model include the effects of interstellar extinction according to the default assumptions included in the web form.

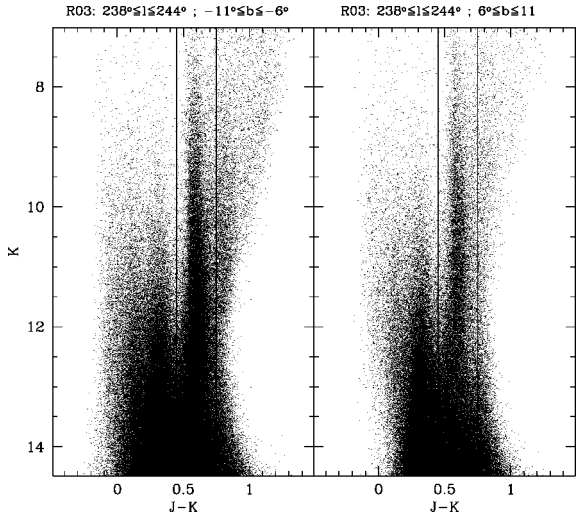

Figure A1. Example of synthetic CMDs extracted from the R03 model. The symbols and the scale are the same as in Fig. 1. The continuous line encloses the colour window $0.45 \leqslant J - K \leqslant 0.70$.

From the observed data set of Fig. 1, we fitted the following relations for the photometric errors in $K(J)$ as a function of – not extinction-corrected – $K(J)$ magnitude:

$$\epsilon K = 0.0236 - 0.00047K + 3.480 \times 10^{-8} \exp(K) \text{ mag}, \quad \text{(A1)}$$

$$\epsilon J = 0.0169 + 0.00024J + 5.840 \times 10^{-9} \exp(J) \text{ mag}. \quad \text{(A2)}$$

To simulate realistically the effect of photometric errors on synthetic stars, we computed ϵK and ϵJ for each of them with the above equations, we randomly extracted a Gaussian deviate (δ, positive or negative, in σ units) for each of them, and then we added the resulting synthetic errors $\delta_K \times \epsilon K$ and $\delta_J \times \epsilon J$ to their K and J magnitudes, respectively. After that, we corrected the synthetic stars for extinction, using the A_V value associated by the model to each star. In the following, J and K stand for extinction-corrected magnitudes, as in the rest of the paper.

The above procedure should provide synthetic samples as similar as possible to the observed ones, including the effect of photometric errors. The comparison of the final synthetic CMDs for the $l = 241^\circ$ window (Southern and Northern hemisphere) shown in Fig. A1 with the observed CMD of Fig. 1 demonstrates that this objective has

[4] See the web form of the R03 model and the explanations provided therein, http://bison.obs-besancon.fr/modele/.

been achieved: the overall similarity between observed and synthetic CMDs is striking. In Fig. A1, we also report the adopted colour window we use to select RC stars in the observed sample. A shift of 0.04 mag in $J - K$ has been applied to all the synthetic samples to centre the vertical plume of RC stars within the selection window, as it is in the observed case. This small mismatch in colour is likely due to a non-perfect match between the theoretical star tracks used by the R03 model and real stars (quite a usual occurrence) as well as to tiny differences in the adopted extinction laws. In any case, the following results are essentially unaffected by the small colour shift applied. In the following, we will consider only synthetic stars falling in our colour-selection window. Hence, when we speak of *dwarfs* we mean stars of class 4 or 5 (R03) having $0.45 \leqslant J - K \leqslant 0.70$, and for *giants* we mean stars of class 3 having $0.45 \leqslant J - K \leqslant 0.70$, that is, the stars that we would have selected as RC stars in our analysis.

Before proceeding with our set of tests, Fig. A1 deserves a few comments. It is quite clear that there is a strong asymmetry between the Southern and the Northern samples: the Southern sample contains many more stars and the difference is particularly evident in the RC plume. This is the effect of the warp included in the model. However, the comparison of the LFs of the observed (Fig. 1, left-hand panel) and of the synthetic (Fig. A1, left-hand panel) Southern samples shown in the right-hand panel of Fig. 1 demonstrates that (i) the R03 model provides an excellent overall representation of the observed distribution of stars in the considered colour window (except for the total normalization, which appears too large by a factor of $\sim$3), and (ii) it still fails to reproduce the strong bump in the observed LF around $K \simeq 13.0$, i.e. the putative RC of CMa. This comparison is fully consistent with the coexistence of the Galactic warp *and* an additional stellar system, CMa. Finally, the excellent agreement between the synthetic and observed LFs outside the $K = 13.0 \pm 0.5$ range seems to confirm that our samples are essentially complete down to $K \sim 14.5$, as stated in Cutri et al. (2003).

In Fig. A2, the fraction of dwarfs falling into our colour-selection as a function of K magnitude (F_D) is shown for the Northern (open squares) and Southern (crosses) samples for the three selected directions. There are several interesting conclusions that can be drawn from this plot.

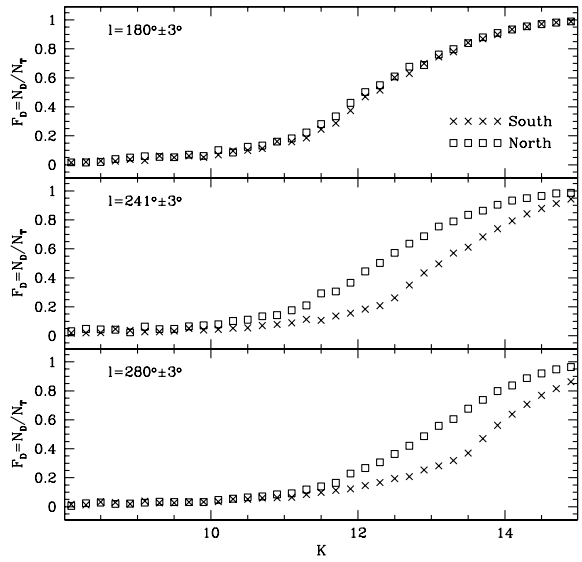

Figure A2. Fraction of dwarf stars in the total number of colour-selected RC stars as a function of K magnitude. The three panels show F_D for three different directions, in the Northern (open squares) and Southern ($\times$symbols) hemispheres.

(i) First of all, since the line of nodes of the warp included in the R03 model lies exactly towards the $l = 180^\circ$ direction, any SN difference in F_D and/or in the detected SN asymmetries in the $l = 180^\circ$ sample must be due to the effect of the $\sim$15 pc displacement of the Sun to the north of the Galactic plane. The upper panel of Fig. A2 shows that difference in F_D is very small, less than 5 per cent in any bin for $K \geqslant 12.0$ and $\simeq$1 per cent in the whole $12.0 \leqslant K \leqslant 14.0$ range. Moreover, the SN difference in giants at $l = 180^\circ$ is 5 per cent of that at $l = 241^\circ$ and 2 per cent of that at $l = 280^\circ$. Finally, the SN difference in the *total* number of colour-selected RC stars at $l = 180^\circ$ is 12 per cent of that at $l = 241^\circ$ and 6 per cent of that at $l = 280^\circ$. The conclusion is that the off-plane position of the Sun has very little effect both on the contamination by dwarfs and on the amplitude of observed SN asymmetries, for the applications considered here. Hence, our decision to neglect it in the analysis described in this paper appears to be fully justified.

(ii) In the range most relevant for the present study ($12.0 \leqslant K \leqslant 14.0$), F_D is quite large, reaching the 80 per cent level at $K = 14.0$ in some cases.

(iii) The overall degree of contamination is quite similar independent of the considered directions, from the anticenter to $l = 280^\circ$.

(iv) There are significant differences in the Northern and Southern F_D towards $l = 241^\circ$ and 280°, up to 20−30 per cent in some bins. However, F_D is *always higher in the Northern hemisphere than in the Southern one*. It appears that, according to the R03 model, NS differences in the contamination by dwarfs are working *against* the detection of real overdensities in the Southern hemisphere.

The latter result may appear puzzling at a first glance, but it can be easily explained by looking into the synthetic samples. It turns out that it is due to the presence of a significant SN asymmetry at large Galactocentric distances (i.e. the warp) that is much larger in giants than in dwarfs, in the magnitude ranges of interest. For example, in the range $12.0 \leqslant K \leqslant 14.0$, at $l = 241^\circ$ the SN ratio of dwarf density is $\rho_D(S)/\rho_D(N) = 29096/24371 = 1.19$ while for giants $\rho_G(S)/\rho_G(N) = 28684/7572 = 3.79$. Therefore, even if there are more dwarfs in the south than in the north, the imbalance in giants is much larger and the final F_D is consequently larger in the north ($F_D = 76$ per cent) than in the south ($F_D = 50$ per cent). At $l = 280^\circ$, $\rho_D(S)/\rho_D(N) = 35427/31333 = 1.13$, while $\rho_G(S)/\rho_G(N) = 70305/22067 = 3.18$, in the same range of magnitudes. This implies that in the presence of a distant SN asymmetry (as the warp, as in the R03 model we are presently considering, or CMa, or both), the observed imbalance in dwarfs is small in this magnitude range, such that the contribution by dwarfs essentially disappears when Southern and Northern counts are subtracted.

The above results drive us to the two key questions we have to answer to really check the reliability of the results of the present paper.

(i) What is the contribution of dwarf contamination to *subtracted densities*?

(ii) Is our observable, the subtracted density of colour-selected RC stars $\rho(S) - \rho(N)$, a good tracer of the real overdensity of giants? In other words, is it a good estimator of the quantity we are interested in $[\rho_G(S) - \rho_G(N)]$?

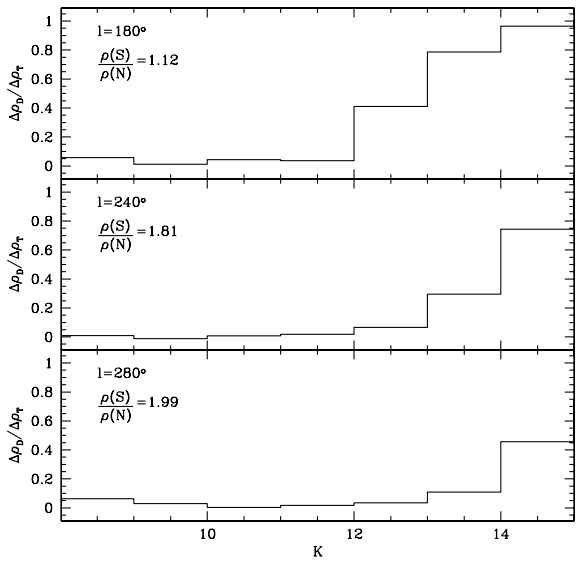

Figure A3. Contribution of the SN imbalance in dwarf stars to the total SN density difference as a function of magnitude, for three different directions. $\rho(S)/\rho(N)$ is the ratio of colour-selected RC stars in the range $12.0 \leqslant K \leqslant 14.0$, and roughly describes the degree of total SN imbalance in each given direction.

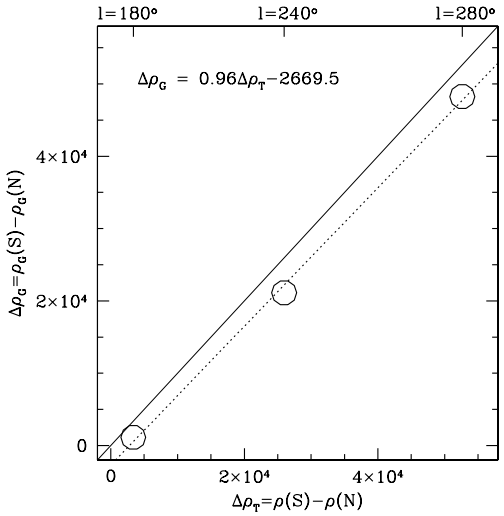

Figure A4. Correlation between the total subtracted density of colour-selected RC stars and the real subtracted density of giants. The continuous line passes through the origin and has slope 1.0, while the dotted line is the best linear fit to the data (see the equation in the upper left-hand corner of the plot). The directions corresponding to the three plotted points are indicated in the upper x-axis.

Fig. A3 answers the first question. There we plot the fraction of the total SN density difference that is due to dwarfs

$$\frac{\Delta\rho_D}{\Delta\rho_{\rm T}} = \frac{\rho_D(S) - \rho_D(N)}{\rho(S) - \rho(N)}$$

as a function of magnitude for the three considered directions. The subscript T stands for Total = dwarfs + giants. The ratio of the total Southern-to-Northern density is also reported within each panel. This plot shows that in absence of a real SN asymmetry [$l = 180^\circ$, $\rho(S)/\rho(N) \sim 1$], the contribution is quite significant (>40 per cent) for $K > 12.0$. On the other hand, towards directions that cross the warp asymmetry [$l = 241^\circ, 280^\circ$, $\rho(S)/\rho(N) > 1.8$] the dwarf contribution remains lower than 30 per cent everywhere, for $K \leqslant 14.0$. Hence, even in a regime of *strong* contamination by dwarfs, the effects on SN subtraction are quite limited for $K \leqslant 14.0$ and in the presence of an overdensity like the warp and/or CMa. On the other hand, our subtracted maps may be significantly affected (or even dominated, in some cases) by dwarf contamination around $l = 180^\circ$ and for $K > 14.0$. It is very interesting to note that in those regions we see a low-significance and smooth SN residual (Fig. 3) that completely disappears when we subtract by the rescaled Northern density map (Fig. 5). On the other hand, all the structured overdensities we deal with in this paper lie in the region where dwarfs provide a minor contribution to the subtracted densities ($l > 200^\circ$ and $K \leqslant 14.0$). Within this context, there is another interesting point worth considering. Since the contribution of dwarfs to our subtracted densities grows continuously with magnitude even for $K \leqslant 14.0$, if our maps were seriously affected by dwarf contamination we would expect to see a corresponding growth of density with heliocentric distance. On the contrary, in the direction of CMa we see *both a growth and a decrease of the density* (see Figs 3 and 5). The distance profile of Fig. 11 shows that towards $l \simeq 240^\circ$ the subtracted density reaches a maximum at $D_\odot = 7.2$ kpc, corresponding to $K = 12.8$, and then essentially falls to zero at $D_\odot \simeq 10.0$ kpc, corresponding to $K = 13.5$, a completely different profile with respect to what is expected from a distribution of Galactic dwarf stars. This occurrence strongly suggests that dwarfs cannot have a major role in determining the observed distribution of the CMa overdensity. The same argument is valid also when considering the trend of contamination of subtracted densities as a function of Galactic longitude. Since the degree of contamination grows towards $l = 180^\circ$, if dwarfs were dominant contributors to the subtracted density we should see the maximum density towards $l = 180^\circ$. On the contrary, the density in that direction is low and smooth, while it is much higher and more strongly peaked towards $l \simeq 240^\circ$.

Fig. A4 tries to answer question (ii), above. This is simply a plot of the SN density difference in the total number of stars selected in colour as RC candidates with our technique (i.e. our observable $\Delta\rho_{\rm T}$) versus the actual difference in the SN density of giants (i.e. the quantity we want to estimate, $\Delta\rho_G$), in the range $12.0 \leqslant K \leqslant 14.0$, for the three directions we are considering. The correlation between $\Delta\rho_{\rm T}$ and $\Delta\rho_G$ is *very strong and essentially linear*. Moreover, the coefficient of the linear best-fitting model is near unity, hence *our observable appears as an excellent estimator of the true SN density difference in giants*, at least in the presence of an asymmetry like the warp embedded in the R03 model.

In summary, based on the above experiments with the R03 Galactic model, we can conclude the following.

(i) The neglection of the displacement of the Sun with respect to the Galactic plane has very little effect on our analysis, and can be safely ignored.

(ii) While our samples of colour-selected RC stars may be heavily contaminated by dwarfs, the effects of the contamination are much lower on the subtracted-density maps. The contribution of dwarfs to the 'observed' $\Delta\rho_{\rm T}$ is lower than 30 per cent for $K \leqslant 14.0$ towards $l = 240^\circ$ and 280°, and much lower than this for $K \leqslant 13.0$. Note that these numbers take into account only the known Galactic components, the presence of an extra asymmetry in the considered range of distances (i.e. CMa; see Fig. 1) would further reduce the rôle of dwarfs.

(iii) The observable we adopt ($\Delta\rho_{\rm T}$) appears to trace very well the true SN imbalance of giants under the realistic conditions provided by the R03 model.

It is conceivable that the CMa overdensity we observe using colour-selected putative RC stars may be in fact produced by an unexpected asymmetry in dwarfs. However, the dwarfs contributing to our counts in the range $12.0 \leqslant K \leqslant 14.0$ have heliocentric distances $0.0\,\mathrm{kpc} \leqslant \mathrm{D}_{\odot} \leqslant 4.5\,\mathrm{kpc}$. Their distance distribution shows a *strong* peak at $\mathrm{D}_{\odot} \simeq 1.0$, the mean is $\langle \mathrm{D}_{\odot} \rangle = 1.0$ kpc and the standard deviation is $\sigma = 0.7$ kpc, and 89 per cent have $\mathrm{D}_{\odot} \leqslant 2.0$ kpc. Hence, a strong and *very compact* clump of dwarfs[5] would have to be present in the Southern hemisphere, at $\sim$1.0 kpc from the Sun towards $l = 240^{\circ}$, a feature that is obviously *not present* in the R03 model. As far as we know, there is no report in the literature of such a local overdensity. Finally, it should be recalled that the position and size of the RC overdensity studied here match very well those derived for CMa with other tracers (M giants and MS stars) that are much less affected by contamination from spurious sources.

[5] Actually, it must be significantly more compact than the distribution of RC stars we attribute to CMa, since the selected dwarfs would span a much larger range of absolute magnitudes, with respect to RC stars.

This paper has been typeset from a TEX/LATEX file prepared by the author.